Available online at www.sciencedirect.com
SCIENCE DIRECT
Journal of Sound and Vibration 294 (2006) 780–806
JOURNAL OF SOUND AND VIBRATION
www.elsevier.com/locate/jsvi

Acoustic scattering by an axially-segmented turbofan inlet duct liner at supersonic fan speeds

A. McAlpine[a,*], R.J. Astley[a], V.J.T. Hii[a], N.J. Baker[b], A.J. Kempton[b]

[a]*Institute of Sound and Vibration Research, University of Southampton, Southampton SO17 1BJ, UK*
[b]*Rolls–Royce plc, Derby, P.O. Box 31, DE24 8BJ, UK*

Received 21 December 2004; received in revised form 1 December 2005; accepted 5 December 2005
Available online 10 March 2006

Abstract

Fan noise is one of the principal noise sources in turbofan aero-engines. At supersonic fan speeds, fan tones are generated by the "rotor-alone" pressure field. In general, these tones can be well absorbed by an inlet duct acoustic liner, except at high supersonic fan speeds when the rotor-alone pressure field is well cut-on. In this article an axially segmented liner is proposed, which is predicted to improve the attenuation of tones at high supersonic fan speeds. The analysis is based on locally reacting cavity liners. The axially segmented liner is axisymmetric and consists of two circular sections of different linings joined together. The optimum design consists of two linings with the same face-sheet resistance, but with different cavity depths. The depth of the liner adjacent to the fan is very thin. This means that where the two liners are joined there is a wall impedance discontinuity that can cause acoustic scattering. Fan tones can be modelled in terms of spinning modes in a uniform circular-section duct. The liner is axisymmetric, so modal scattering will be only between different radial modes. The optimum design minimizes the acoustic energy scattered into the first radial mode. This improves the attenuation of fan tones at high supersonic fan speeds, because acoustic energy is scattered into high radial mode orders, which are better absorbed by the lining.
© 2006 Elsevier Ltd. All rights reserved.

1. Introduction

The sound that propagates in an aircraft turbofan inlet duct is almost entirely due to the fan. Fan tone noise is highly dependent on the engine power, or fan speed. At subsonic fan speeds, the "rotor-alone" pressure field attached to the ducted fan is cut-off. The dominant fan tones are harmonics of the blade passing frequency (BPF), which are generated by rotor–stator interactions, and other similar mechanisms such as interaction with mean-flow distortion and scattering by liner discontinuities.

On a typical modern high bypass ratio turbofan engine the fan tip speed will be supersonic at high engine powers, for example at the engine "cutback" and "sideline" operating conditions (nominally about 80–85 and 90–95% fan speed). At supersonic fan speeds, the rotor-alone pressure field is not cut-off. Fan tones which are harmonics of the engine shaft rotation frequency, or engine orders (EO), are generated by the rotor-alone

*Corresponding author. Tel.: +44 23 8059 2291; fax: +44 23 8059 3190.
E-mail address: am@isvr.soton.ac.uk (A. McAlpine).

0022-460X/$ - see front matter © 2006 Elsevier Ltd. All rights reserved.
doi:10.1016/j.jsv.2005.12.039

Nomenclature

A	modal amplitude (Pa)
b	duct radius (m)
B	number of fan blades
BPF	blade passing frequency (Hz)
c	speed of sound ($\mathrm{m\,s^{-1}}$)
d	distance between fan plane and liner (m)
EO	engine order
f	frequency (Hz)
$\mathscr{F}$	engine shaft rotation frequency (Hz)
h	liner depth (m)
I_x	axial intensity ($\mathrm{W\,m^{-2}}$)
Im{}	denotes imaginary part
J_m	Bessel function of the first kind, order m
k	acoustic wavenumber ($\mathrm{rad\,m^{-1}}$)
kb	Helmholtz number (non-dimensional frequency)
k_x	axial wavenumber ($\mathrm{rad\,m^{-1}}$)
l	liner length (m)
L	duct length (m)
max{}	denotes maximum value
(m,n)	(azimuthal, radial) mode order
M_x	axial Mach number
N	number of radial modes used in mode-matching
n_c	highest cut-on radial mode order (m and ω fixed)
p	pressure (Pa)
PWL	sound power level (dB)
r	radial coordinate (m)
rev/min	revolutions per minute
R	resistance (non-dimensional)
Re{}	denotes real part
SPL	sound pressure level (dB)
t	time (s)
U	axial mean flow ($\mathrm{m\,s^{-1}}$)
W	sound power (W)
x	axial distance upstream of the fan (m)
X_c	cavity reactance (non-dimensional)
Z	specific acoustic impedance (non-dimensional)

Greek letters

α_x	axial wavenumber, lined duct section II ($\mathrm{rad\,m^{-1}}$)
β_x	axial wavenumber, lined duct section III ($\mathrm{rad\,m^{-1}}$)
Δ_{LAM}	least attenuated mode transmission loss (dB)
Δ_{PWL}	sound power transmission loss (dB)
ζ	cut-off ratio
η	radial wavenumber, lined duct section III ($\mathrm{rad\,m^{-1}}$)
θ	azimuthal coordinate (rad)
θ_x	mode angle (rad)
κ	radial wavenumber ($\mathrm{rad\,m^{-1}}$)
λ	acoustic wavelength (m)
μ	radial wavenumber, lined duct section II ($\mathrm{rad\,m^{-1}}$)
ρ	density ($\mathrm{kg\,m^{-3}}$)
ω	angular frequency $2\pi f$ ($\mathrm{rad\,s^{-1}}$)

Subscripts

1	denotes first lined segment (duct section II)
2	denotes second lined segment (duct section III)
m,n	mode (m,n)
0	mean value

Superscripts

$'$	denotes an acoustic quantity
$\hat{}$	denotes a harmonic quantity
$+$	denotes a right-running mode
$-$	denotes a left-running mode
I	rigid duct section, adjacent to the fan plane
II	first lined duct segment
III	second lined duct segment
IV	rigid duct section, adjacent to the exit plane

pressure field. The name "buzz-saw" noise or multiple pure tones is generally used to describe this component of fan noise. At source, i.e. close to the fan, the BPF harmonics are the dominant tones in the EO spectrum, although the principal source generation mechanisms at subsonic and supersonic fan speeds are in fact different.

Turbofan inlet ducts are lined with a sound absorbent acoustic lining to reduce noise emissions. The type of acoustic liners are typically locally reacting cavity linings. The specific acoustic impedance of these type of liners depends on the properties of the lining, the mean flow and the frequency of the sound. In general, it is

more difficult to attenuate the fan tones as the engine power is increased, notably at high supersonic fan speeds. (The reasons for this are outlined in Section 2.)

A potential method to improve the attenuation at high supersonic fan speeds is to try to alter the sound field. In this article a non-uniform "axially segmented" liner is proposed. The liner is a two-section segmented liner, which is axisymmetric. It consists of two circular sections of different linings joined together. The aim is to introduce a wall impedance discontinuity that causes additional acoustic scattering, which may increase the sound attenuation.

Modelling transmission and radiation of sound in ducts is reviewed by Eversman [1]. Most inlets are nearly circular, and are smoothly contoured so that the aerodynamic flow is stable, and total pressure losses are small. At the typical BPF, the acoustic wavelength is of the order of one-tenth of the inlet duct diameter, so changes in the inlet's diameter, and also the mean flow, are generally assumed to be small, at least over an acoustic wavelength. Also, in Ref. [2] it is shown that solutions of sound transmission in a duct with a thin shear layer at the wall, and sound transmission with a uniform flow and continuity of particle displacement applied at the wall, converge in the limit as the shear layer thickness tends to zero. Therefore, to a first approximation, here an inlet is modelled as a uniform circular-section duct containing a uniform mean-flow. This permits the sound field to be represented in terms of "spinning" modes, which can be expressed in terms of known analytic functions [3].

Recently, there has been renewed interest in modelling, using analytic methods, sound transmission in slowly-varying ducts [4]. However, computational techniques, such as the finite element method, are generally required to examine more complex non-uniform duct geometries and mean flows [5]. In this article, a uniform circular-section duct and uniform flow is assumed, in order that all the analysis may be carried out in terms of spinning modes.

The concept of non-uniform liners has been studied in the past. In the 1970s and early 1980s there was interest in the use of multi-section axisymmetric lined ducts to suppress inlet noise.[1] Refs. [7–10] are examples of the work at this time. Lansing and Zorumski [7] appears to be the first published work on the type of axially segmented liner which is examined in this current article. Unruh [8] first examined how the liner's length, as well as its impedance, may be tuned to optimize the attenuation. Also, both Baumeister [9] and Tsai [10] realized that the first segment of lining acts as a scatterer, which facilitates the attenuation of the sound in adjacent lined segments. However, Ref. [9] concluded that 'the use of optimized axially segmented liners fails to offer sufficient advantage over a uniform liner to warrant their use except in low-frequency, single-mode application'.

In this article a simple design of an axially segmented liner is proposed, which is predicted to increase significantly, compared to a typical uniform liner design, the attenuation of the BPF tone at high supersonic fan speeds. This is not a low-frequency application, but owing to the nature of the source, it may be viewed as a type of single-mode application. The type of axially segmented liner proposed in this article is the subject of European Patent No. EP1411225 [11].

2. Scattering by an axially segmented liner

The inlet duct geometry used here is shown sketched in Fig. 1. Take cylindrical polar co-ordinates (r, θ, x) such that the centre of the duct is aligned with the x-axis, the fan plane is at $x = 0$, the exit plane is at $x = L$, and the duct wall is at $r = b$. The duct is lined from $x = d$ to $d + l$. The flow is assumed uniform across the duct cross-section, and has axial Mach number $M_x = U_0/c_0$.

The sound field in a waveguide or duct is commonly expressed in terms of modes. Assume that for a harmonic noise source, with frequency ω, the harmonic pressure field $p'(r, \theta, x, t) = \hat{p}(r, \theta, x)\exp(\mathrm{i}\omega t)$ satisfies the convected Helmholtz equation

$$\left(\mathrm{i}k + M_x \frac{\partial}{\partial x}\right)^2 \hat{p} = \nabla^2 \hat{p}, \quad k = \omega/c_0. \tag{1}$$

[1]Also, at this time there was work on peripherally varying liners which is discussed in more detail in Ref. [6].

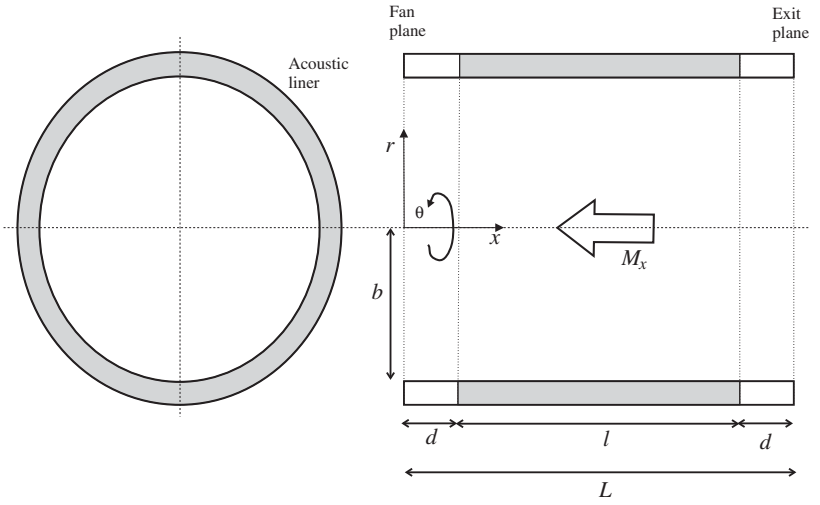

Fig. 1. Inlet duct geometry.

It is well known, (e.g. as shown by Eversman [1]), that on separating the variables r, θ and x modal solutions of Eq. (1) can be expressed as

$$\begin{aligned}\hat{p}(r,\theta,x) &= \sum_{m=-\infty}^{\infty}\sum_{n=1}^{\infty}(\hat{p}^{+}_{m,n}+\hat{p}^{-}_{m,n})\\ &= \sum_{m=-\infty}^{\infty}\sum_{n=1}^{\infty}(A^{+}_{m,n}J_m(\kappa^{+}_{m,n}r)\mathrm{e}^{\mathrm{i}(m\theta-k^{+}_{x\,m,n}x)}+A^{-}_{m,n}J_m(\kappa^{-}_{m,n}r)\mathrm{e}^{\mathrm{i}(m\theta-k^{-}_{x\,m,n}x)}),\end{aligned} \tag{2}$$

where

$$k^{\pm}_{x\,m,n}=\frac{k}{1-M_x^2}\left(-M_x\pm\sqrt{1-(1-M_x^2)\left(\frac{\kappa^{\pm}_{m,n}}{k}\right)^2}\right). \tag{3}$$

Each mode is identified by its azimuthal and radial order, m and n, denoted by subscript m,n. Note that $+,-$ denote right- and left-running modes respectively.

In a rigid-walled duct, at a fixed frequency, only a finite number of modes can propagate inside the duct and transmit acoustic power. All the remaining modes will be "cut-off" and transmit no acoustic power. The cut-off ratio $\zeta_{m,n}$ is defined as

$$\zeta_{m,n}=\frac{kb}{\kappa_{m,n}b\sqrt{1-M_x^2}}. \tag{4}$$

Mode (m,n) propagates inside the duct, or is "cut-on", if $\zeta_{m,n}>1$ (in which case the axial decay rate $\mathrm{Im}\{k_{x\,m,n}\}$ is zero), otherwise it is cut-off. For each azimuthal mode order m, the radial modes are ordered in terms of decreasing cut-off ratio, i.e. $\zeta_{m,1}>\zeta_{m,2}>\zeta_{m,3}\ldots$, which is equivalent to ordering the modes in terms of increasing $\mathrm{Re}\{\kappa_{m,n}\}$. Radial mode orders with $n>n_c$ are all cut-off.

Geometric acoustics can be used to model sound propagation in a duct, in terms of rays being reflected between the duct walls. For example, in a two-dimensional duct with parallel walls, the duct modes can be expressed exactly as the superposition of two plane waves.[2] The angle between the component waves

[2]In a circular duct the ray structure of the duct modes is described in Ref. [12].

of the mode and the duct axis is known as the axial mode angle θ_x. The cut-off ratio ζ and mode angle θ_x are linked. For example, without flow it is straightforward to show that $\sin\theta_x = 1/\zeta$.[3] Modes near cut-off ($\zeta \approx 1$) have mode angles close to 90°, whereas modes that are well cut-on have smaller mode angles.

In an acoustically lined duct, all the modes have complex radial and axial wavenumbers. There is no unique method to order the modes because all the radial wavenumbers are complex. However, it is still logical to order the radial modes the same as in a rigid duct. It will be useful to extend the normal use of the terms "cut-on" and "cut-off" also to describe modes in a lined duct. Modes which are cut-off ($\zeta < 1$), or near cut-off ($\zeta \approx 1$), will have large axial decay rates in a lined duct. Conversely, propagating modes which are well cut-on will have small axial decay rates.

The mode angle concept is useful to illustrate the different attenuation rates in a lined duct.[4] The component waves of modes near cut-off (with mode angles close to 90°) are reflected a large number of times per unit length as they propagate in the duct, whilst the component waves of well cut-on modes are reflected fewer times per unit length. The attenuation per unit length will depend on the number of reflections, as well as the frequency of the sound, and the properties of the acoustic lining, so modes near cut-off are generally well absorbed in a lined duct.

Tones and broadband noise can be modelled by modes. In terms of modes, a tone is usually represented by a small number of modes which are linked: for example, modes with the same azimuthal mode order. Broadband noise is usually modelled by a multi-mode source with equal energy per mode.

At subsonic fan speeds, Tyler and Sofrin [3] have shown that the BPF tone, owing to rotor–stator interactions, will be comprised of a combination of spinning modes with different azimuthal and radial mode orders. The azimuthal mode orders depend on the number of fan rotor blades and stator vanes.

At supersonic fan speeds, the rotor-alone pressure field is steady in the rotor's frame of reference, and consists of modes spinning with the same circumferential phase speed as the fan, which equals $2\pi\mathscr{F}$. The circumferential phase speed of a spinning mode is ω/m. Therefore, a rotor-alone tone with frequency $m \times \mathscr{F}$ can be modelled by spinning modes with azimuthal mode order m.[5] The rotating fan's circumferential phase speed will be supersonic only over a small spanwise section of the blade, close to the blades' tips. It follows that at the fan plane most of the acoustic energy will be contained in modes with radial mode order $n = 1$. This means that the fan tonal noise source can be modelled, at frequency $m\mathscr{F}$, by the rotor-alone mode $(m, 1)$. In this article, it is assumed that the BPF tone can be modelled by a single mode, namely the rotor-alone BPF mode $(B, 1)$.

At low supersonic fan speeds, e.g. cut-back, the rotor-alone pressure field is near cut-off. The component waves of the modes will be reflected a large number of times between the duct walls. However, at high supersonic fan speeds, e.g. sideline, the rotor-alone field is well cut-on. It is more difficult to attenuate the rotor-alone modes, as the waves will be only reflected a small number of times between the duct walls.

Rice [14] found that a thin cavity lining better damps well cut-on modes, but modes near cut-off are better damped by a thicker lining. An axially segmented liner can make use of linings of different depths. Also, at supersonic fan speeds, each EO tone can be modelled as a single mode. Therefore, following Baumeister [9], an axially segmented liner should provide a benefit over a uniform liner for the high supersonic fan speed application.

The axially segmented liner is axisymmetric. This is crucial to ensure that for each azimuthal mode order, any scattering is between only radial modes. The aim is to scatter energy into higher radial mode orders, i.e. $n > 1$, which should increase the attenuation because higher-order modes are nearer cut-off.

In this article, in order to assess an axially segmented liner, the predicted sound power transmission loss, at BPF, is used as a metric to optimize the liner's design. The transmission loss is then compared with the predicted attenuation for a uniform liner. The analysis is conducted by using the well known mode-matching technique.

[3]Note that with flow an additional 'mode angle' which includes the convective effect of the mean flow also can be defined, see Ref. [13].

[4]Strictly the mode angles defined in Ref. [13] are based on a rigid circular duct.

[5]EO denotes the non-dimensional frequency of the mth harmonic, i.e. EO $= m\mathscr{F}/\mathscr{F} = m$.

3. Mode-matching technique

In a duct, acoustic scattering can be caused by changes in the impedance of the duct wall. Fig. 2 illustrates the mode-matching technique applied to both an axially segmented and a uniform liner. Details of similar mode-matching schemes can be found in Refs. [15, Chapter 2] and also in Refs. [7,8].

The analysis is outlined for an axially segmented liner. For a uniform liner region II is omitted in the analysis. The harmonic pressure field in the rigid and lined duct sections is expressed as a superposition of Fourier–Bessel modes, consisting of right-running (+) and left-running (−) modes. For azimuthal mode order m,

$$\hat{p}_m^{\mathrm{I}}(r,\theta,x)=\sum_{n=1}^{N}(A_{m,n}^{\mathrm{I}+}J_m(\kappa_{m,n}^{+}r)\mathrm{e}^{-\mathrm{i}k_{x\,m,n}^{+}x}+A_{m,n}^{\mathrm{I}-}J_m(\kappa_{m,n}^{-}r)\mathrm{e}^{-\mathrm{i}k_{x\,m,n}^{-}x})\mathrm{e}^{\mathrm{i}m\theta}, \tag{5}$$

$$\hat{p}_m^{\mathrm{II}}(r,\theta,x)=\sum_{n=1}^{N}(A_{m,n}^{\mathrm{II}+}J_m(\mu_{m,n}^{+}r)\mathrm{e}^{-\mathrm{i}\alpha_{x\,m,n}^{+}x}+A_{m,n}^{\mathrm{II}-}J_m(\mu_{m,n}^{-}r)\mathrm{e}^{-\mathrm{i}\alpha_{x\,m,n}^{-}x})\mathrm{e}^{\mathrm{i}m\theta}, \tag{6}$$

$$\hat{p}_m^{\mathrm{III}}(r,\theta,x)=\sum_{n=1}^{N}(A_{m,n}^{\mathrm{III}+}J_m(\eta_{m,n}^{+}r)\mathrm{e}^{-\mathrm{i}\beta_{x\,m,n}^{+}x}+A_{m,n}^{\mathrm{III}-}J_m(\eta_{m,n}^{-}r)\mathrm{e}^{-\mathrm{i}\beta_{x\,m,n}^{-}x})\mathrm{e}^{\mathrm{i}m\theta}, \tag{7}$$

$$\hat{p}_m^{\mathrm{IV}}(r,\theta,x)=\sum_{n=1}^{N}(A_{m,n}^{\mathrm{IV}+}J_m(\kappa_{m,n}^{+}r)\mathrm{e}^{-\mathrm{i}k_{x\,m,n}^{+}x}+A_{m,n}^{\mathrm{IV}-}J_m(\kappa_{m,n}^{-}r)\mathrm{e}^{-\mathrm{i}k_{x\,m,n}^{-}x})\mathrm{e}^{\mathrm{i}m\theta}. \tag{8}$$

Note that the radial and axial wavenumbers in the rigid duct sections (I, IV) are denoted by κ and k_x, and in the lined duct sections (II, III) by μ,η and α_x,β_x, respectively. Also, in a rigid-walled duct $\kappa_{m,n}^{+}=\kappa_{m,n}^{-}$. The wavenumbers are calculated numerically by using the solution method described by Eversman [1, pp. 122–126]. A brief outline of the procedure used here to calculate modes in a lined duct is in Appendix C.

With uniform flow, Rienstra [16] has shown that up to four surface wave modes may be found. One of these modes may in fact be unstable, similar to the classical Helmholtz instability. This instability mode is usually omitted when using mode-matching. In all the simulations here the instability mode is not included in Eqs. (6) or (7).

The series are truncated at $n=N$. It is crucial that $N>n_c$. Typically, in order to improve the accuracy of the matching, more cut-off modes should be included, so that the near field in the vicinity of each matching plane is accurately modelled. In practice if $n_c\leq 5$, then $N>20$ appears sufficient.

The axial acoustic particle velocity in each duct section can be also expressed as a superposition of Fourier–Bessel modes, similar to Eqs. (5)–(8) but with different $A_{m,n}$'s. By using the acoustic momentum equation it is straightforward to show that

$$\hat{u}_{x\,m,n}^{\pm}=\frac{\xi_{m,n}^{\pm}\hat{p}_{m,n}^{\pm}}{\rho_0 c_0}. \tag{9}$$

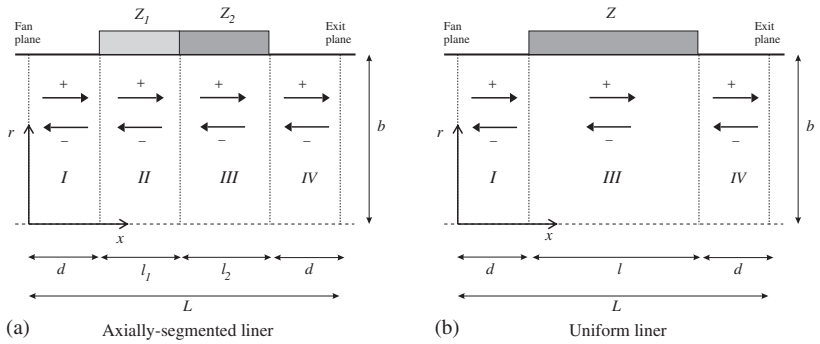

Fig. 2. Inlet duct geometry. Mode-matching technique.

In a rigid duct

$$\xi^{\pm}_{m,n} = \frac{k_{x^{\pm}_{m,n}}}{k - k_{x^{\pm}_{m,n}} M_x}. \tag{10}$$

In the lined duct sections $k_{x_{m,n}}$ in Eq. (10) is replaced by $\alpha_{x_{m,n}}$ or $\beta_{x_{m,n}}$.

The modal amplitudes, $A^{\mathrm{I}+}_{m,n}$, specify the noise source at the fan plane, $x = 0$, which is assumed to be known. It is also assumed that at the exit plane, $x = L$, there is an anechoic termination, which means that $A^{\mathrm{IV}-}_{m,n} = 0$, $n = 1$ to N. In order to evaluate the other modal amplitudes, the pressure and axial particle velocity are matched at $x = d$, $d + l_1$ and $d + l_1 + l_2$ $(= d + l)$.

The Galerkin method of weighted residuals is used for the matching. (This procedure is explained in Ref. [8, p. 7].) For example, continuity of pressure and axial particle velocity at $x = d$ gives

$$\int_{r=0}^{b} rJ_m(\kappa_{m,n} r)\left\{\hat{p}^{\mathrm{II}}_m(r,\theta,d^+) - \hat{p}^{\mathrm{I}}_m(r,\theta,d^-)\right\} \mathrm{d}r = 0, \quad n = 1 \text{ to } N, \tag{11}$$

$$\int_{r=0}^{b} rJ_m(\kappa_{m,n} r)\left\{\hat{u}^{\mathrm{II}}_{x\,m}(r,\theta,d^+) - \hat{u}^{\mathrm{I}}_{xm}(r,\theta,d^-)\right\} \mathrm{d}r = 0, \quad n = 1 \text{ to } N. \tag{12}$$

Similar expressions are formulated for the continuity of pressure and axial particle velocity at $x = d + l_1$ and $d + l_1 + l_2$. This leads to $6N$ sets of equations which can be used to evaluate the $6N$ unknown coefficients. In order to solve the problem using an iterative scheme it is convenient to arrange the equations as follows:

$$\begin{bmatrix} A^{\mathrm{II}+}_{m,n} \\ \hline A^{\mathrm{I}-}_{m,n} \end{bmatrix} = T^1 D^1 \begin{bmatrix} A^{\mathrm{I}+}_{m,n} \\ \hline A^{\mathrm{II}-}_{m,n} \end{bmatrix}, \tag{13}$$

$$\begin{bmatrix} A^{\mathrm{III}+}_{m,n} \\ \hline A^{\mathrm{II}-}_{m,n} \end{bmatrix} = T^2 D^2 \begin{bmatrix} A^{\mathrm{II}+}_{m,n} \\ \hline A^{\mathrm{III}-}_{m,n} \end{bmatrix}, \tag{14}$$

$$\begin{bmatrix} A^{\mathrm{IV}+}_{m,n} \\ \hline A^{\mathrm{III}-}_{m,n} \end{bmatrix} = T^3 D^3 \begin{bmatrix} A^{\mathrm{III}+}_{m,n} \\ \hline A^{\mathrm{IV}-}_{m,n} \end{bmatrix}. \tag{15}$$

T^1, T^2 and T^3 are transfer matrices which relate the pressure and axial particle velocity between adjacent sections of the duct. The coefficients T^1_{ij}, T^2_{ij} and T^3_{ij} are all constant. Their values are listed in Appendix A. D^1, D^2, D^3 are diagonal matrices. The coefficients D^1_{ii}, D^2_{ii} and D^3_{ii} depend on the axial decay rates in each section of the duct. Their values are listed in Appendix B. In Ref. [17], a simple iterative scheme which can be used to solve Eqs. (13)–(15) is outlined.

In the rigid duct sections, the sound power is the sum of the power in all the cut-on modes. The power in each mode can be summed because the mode shapes are orthogonal. The modal sound power $W^{\pm}_{m,n}$ is given by

$$W^{\pm}_{m,n} = 2\pi \int_{r=0}^{b} I_{x^{\pm}_{m,n}} r \,\mathrm{d}r, \tag{16}$$

i.e. the integral of the modal acoustic intensity $I_{x^{\pm}_{m,n}}$ in the $\pm x$-direction over the cross-sectional area of the duct. The form of the axial acoustic intensity is given by Morfey [18, Eq. (16), p. 39]. This leads to

$$W^{\pm}_{m,n} = |A^{\pm}_{m,n}|^2 \chi^{\pm}_{m,n}, \tag{17}$$

where

$$\chi^{\pm}_{m,n} = \frac{\pi b^2}{2\rho_0 c_0} |J_m(\kappa_{m,n} b)|^2 \left[1 - \left(\frac{m}{\kappa_{m,n} b}\right)^2\right] [(1 + M_x^2)\mathrm{Re}\{\xi^{\pm}_{m,n}\} + M_x(1 + |\xi^{\pm}_{m,n}|^2)]. \tag{18}$$

Table 1
Inlet duct specification

Number of fan blades	B	24
Duct radius	b	1.0 m
Duct length	L	1.1 m
Liner length	l	0.8 m
Rigid-walled section	d	0.15 m

Table 2
Fan operating condition

Fan speed	M_x	M_t	BPF	kb	$\zeta_{B,1}$
Sideline	−0.50	1.29	1680 Hz	31.0	1.36

At the fan plane it is assumed that all the acoustic energy is contained in the first radial mode order.[6] Thus, here the sound power transmission loss, at BPF, is defined as

$$\Delta_{\mathrm{PWL}} = 10\log_{10}\frac{W^{\mathrm{I}+}_{B,1}}{\sum_{n=1}^{n_c} W^{\mathrm{IV}+}_{B,n}}. \tag{19}$$

4. Results

The objective is to design a two-section axially segmented liner that is predicted to increase, compared with a uniform liner, the sound power transmission loss Δ_{PWL} of the rotor-alone BPF mode $(B,1)$ at high supersonic fan speeds.

The dimensions of the inlet duct and flow speed used here are realistic for a modern turbofan aero-engine. The inlet duct geometry is listed in Table 1. The fan operating condition is listed in Table 2. The nominal high engine power is referred to as the "sideline" fan speed. Note that at this fan speed, the cut-off ratio of the BPF mode is $\zeta_{B,1} = 1.36$, and two radial modes are cut-on.

The acoustic liners are assumed to be locally reacting cavity linings. These consist of a porous facing-sheet (with resistance R) and a rigid back plate, which sandwich a honeycomb separator with cavity depth h. The non-dimensional specific acoustic impedance[7] is given by

$$Z = R + \mathrm{i}\,X_c = R - \mathrm{i}\cot(kh). \tag{20}$$

A uniform liner is shown sketched in Fig. 2(b). It is straightforward to optimize a uniform liner. The objective function is Δ_{PWL}. The design variables are R and h. The maximum and minimum permitted values of R and h are prescribed. Then, the design space (R,h) is searched to locate $\max\{\Delta_{\mathrm{PWL}}\}$.

A two-section axially segmented liner is shown sketched in Fig. 2(a). The two lined segments have lengths l_1 and l_2, and specific acoustic impedances Z_1 and Z_2. Note that subscript 1 denotes the first lined segment, and subscript 2 denotes the second lined segment. In this case the objective function Δ_{PWL} will depend on five design variables. These are the face-sheet resistance and cavity depth of each liner, R_1, h_1 and R_2, h_2, and the length l_1. The total length of the liner l is fixed, i.e. $l_1 + l_2 = l$. In this case the design space $(R_1, h_1, R_2, h_2, l_1)$ is searched to locate $\max\{\Delta_{\mathrm{PWL}}\}$.

[6]In this article all the mode-matching calculations are for a single right-running mode at $x = 0$. It is straightforward to include more than one incident mode, but the results will then depend on the phasing of the multiple incident modes.

[7]In order to simplify the liner optimization the mass reactance is assumed to be zero. Also, the acoustic impedance has been non-dimensionalized by dividing by $\rho_0 c_0$, ($c_0 = 340\,\mathrm{m\,s^{-1}}$ and $\rho_0 = 1.2\,\mathrm{kg\,m^{-3}}$).

4.1. Uniform liner

Fig. 3(a) shows Δ_{PWL} contours plotted in the (R,h)-plane. R varies between 0.5 and 10, and h varies between 1 and 100 mm. There is a local maximum point at $R = 6.5$, $h = 20$ mm.

However, in practice a lining with a resistance as high as 6.5 is unlikely to be used. A lower resistance would be more effective at lower fan speeds, and to absorb broadband noise. Fig. 3(b) shows how Δ_{PWL} varies with h when $R = 3$. This is a more realistic value of the resistance. Cavity depths, ranging from about 5 to 60 mm, are predicted to attenuate the BPF tone by a similar amount, with $\max\{\Delta_{\mathrm{PWL}}\}$ about 14 dB.

4.2. Axial liner

The design space is constrained, so that only realistic values for a turbofan inlet liner are included. In this case R_1, R_2 vary between 1 and 3, and h_1, h_2 vary between 0 and 50 mm. The length l_1 can vary from 0 to l (= 0.8 m); $l_1 = 0$ and $l_1 = l$ are both special cases that correspond to uniform liner designs. With five design variables it is still possible to generate contour plots which illustrate where maximum points are located in the $(R_1, h_1, R_2, h_2, l_1)$-space.

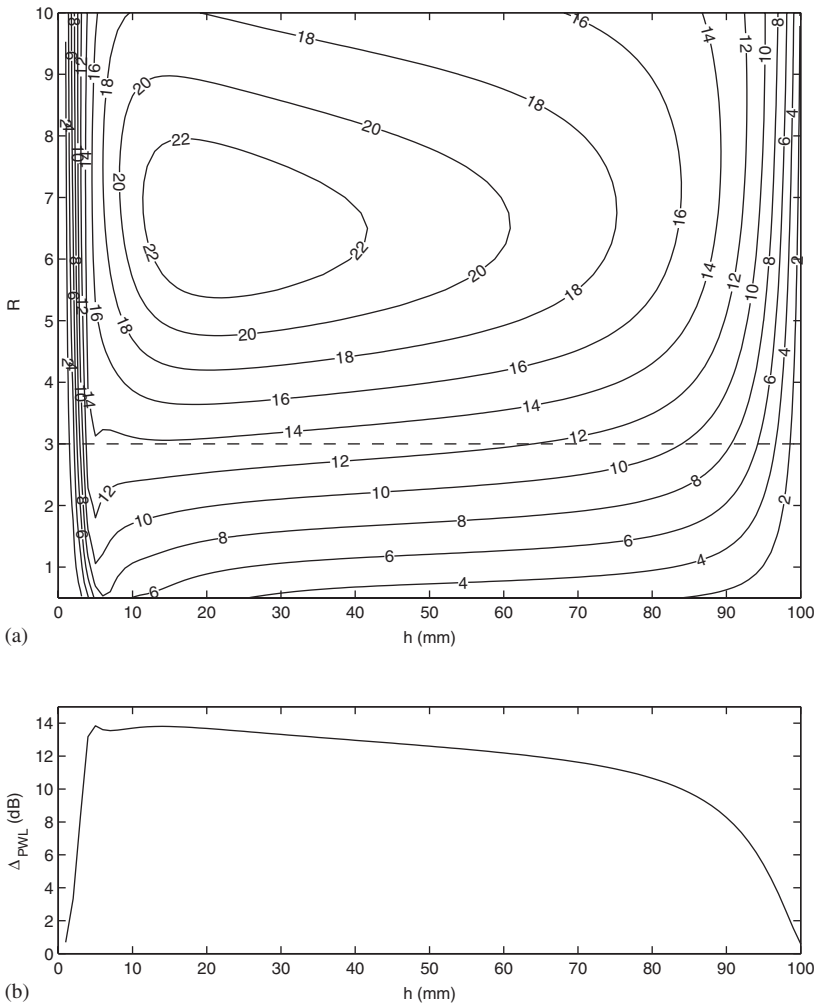

Fig. 3. Predicted sound power transmission loss at blade passing frequency for the uniform liner: (a) Resistance $R = 0.5-10$, and liner depth $h = 0-100$ mm. Contour lines are Δ_{PWL} (in dB). (b) $R = 3$ (fixed), and $h = 0-100$ mm.

An example of the axially segmented liner optimization results is shown in Fig. 4. The figure contains nine subplots. Each subplot shows Δ_{PWL} contours plotted in the (h_1, h_2)-plane, with R_1, R_2 and l_1 fixed. The horizontal axis (h_1) and vertical axis (h_2) vary from 0 to 50 mm. The values of the face-sheet resistances R_1 and R_2 can be read from the main axes. The value of l_1 is fixed. In this example the ratio $l_1/l = 0.3$. Similar figures were obtained for different ratios of l_1/l between 0 and 1, but the highest values of Δ_{PWL} were found when l_1/l is close to 0.3.

In Fig. 4 in each subplot there are two local maximum points. In general, the largest values of Δ_{PWL} are found with the maximum prescribed values of the resistance. In Fig. 5 there is an enlarged version of the contour subplot with $R_1 = R_2 = 3$. In this case the local maximum points are located at $h_1 = 3\,\mathrm{mm}, h_2 = 7\,\mathrm{mm}$ and $h_1 = 5\,\mathrm{mm}, h_2 = 35\,\mathrm{mm}$. The first point is not considered here because both liner segments are thin. A thicker liner would be more effective at lower fan speeds, and to absorb broadband noise. However, the second point could provide a practical design, because it combines a thin lined segment with a thicker lined segment. In fact, the thicker liner of depth 35 mm is a more typical thickness of the type of cavity linings used in inlet ducts. Also, in Fig. 3(b) it can be seen that if $R = 3$, then a uniform liner of depth $h = 35\,\mathrm{mm}$ is close to the optimum uniform lining.

The importance of length l_1 is seen in Fig. 6, which shows how Δ_{PWL} varies with l_1, when $R_1 = 3$, $h_1 = 5\,\mathrm{mm}$, and $R_2 = 3$, $h_2 = 35\,\mathrm{mm}$. The choice of length l_1 is crucial. In this example, $\max\{\Delta_{\mathrm{PWL}}\}$ is predicted when $l_1 = 0.23\,\mathrm{m}$, which is very close to $l_1/l = 0.3$.

When the values of the face-sheet resistance are constrained to be $R \leq 3$, the optimum axially segmented liner design is $R_1 = 3, h_1 = 5\,\mathrm{mm}, R_2 = 3, h_2 = 35\,\mathrm{mm}$ and $l_1 = 0.23\,\mathrm{m}$. In this case, $\max\{\Delta_{\mathrm{PWL}}\} = 38.1\,\mathrm{dB}$. As a more advanced optimization method is not used, the optimum design may not in fact be the global optimum. A preliminary attempt at using more advanced optimization methods for this type of problem is in Ref. [19]. For a uniform liner, with $R = 3$ and $h = 35\,\mathrm{mm}$, i.e. the same lining as the second segment of the axially segmented liner, $\Delta_{\mathrm{PWL}} = 13.1\,\mathrm{dB}$. A three-fold increase in the sound power transmission loss at BPF is predicted with the axially segmented liner, compared with a typical uniform liner of the same length. These proposed designs are shown sketched in Fig. 7.

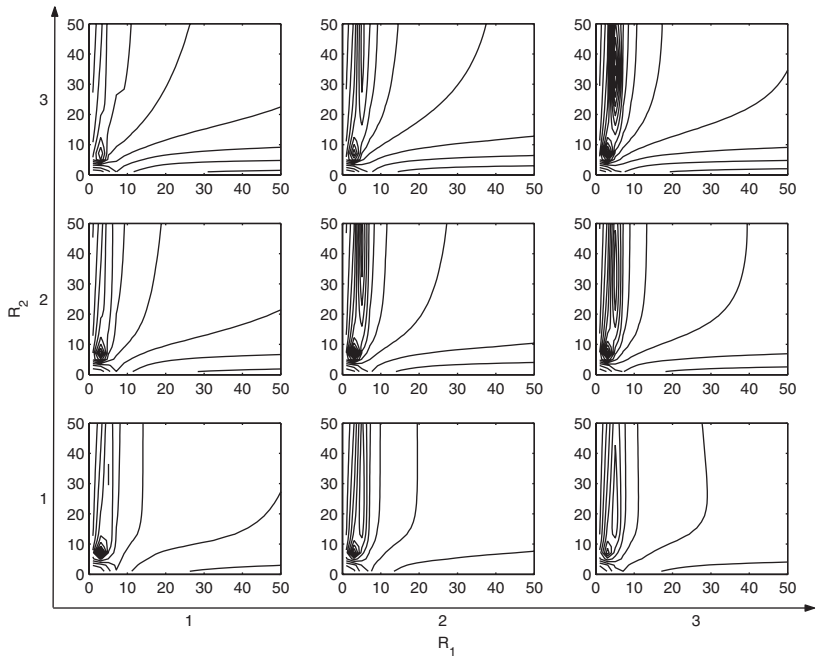

Fig. 4. Predicted sound power transmission loss at blade passing frequency for the axially segmented liner, with $l_1 = 0.3\,l$. Contour lines are Δ_{PWL} (in dB). Each subplot shows Δ_{PWL} contours with R_1, R_2 fixed (= 1, 2 or 3), and h_1 (horizontal axis) and h_2 (vertical axis) from 0 to 50 mm.

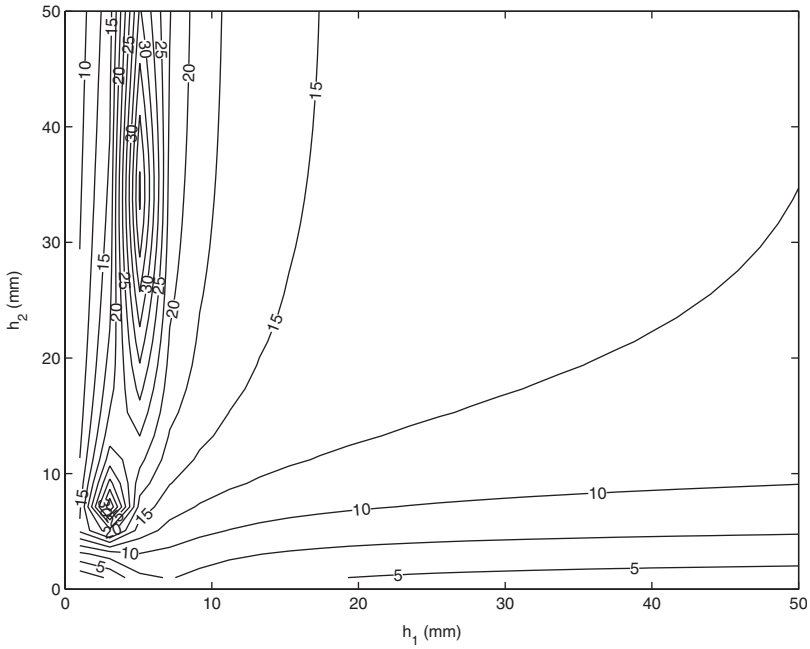

Fig. 5. Predicted sound power transmission loss at blade passing frequency for the axially segmented liner, with $l_1 = 0.3\,l$, and $R_1 = R_2 = 3.0$. Contour lines are Δ_{PWL} (in dB).

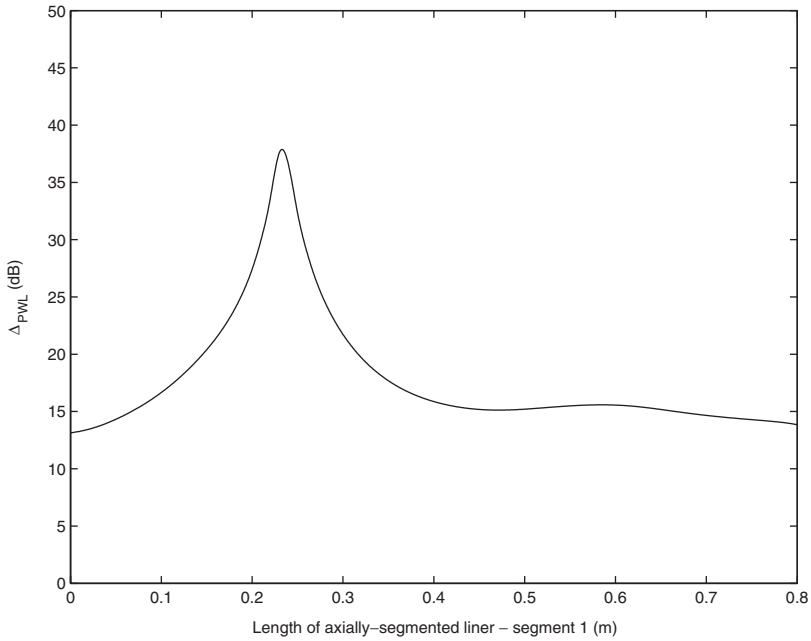

Fig. 6. Predicted sound power transmission loss at blade passing frequency for the axially segmented liner, with $R_1 = R_2 = 3.0$, $h_1 = 5\,\mathrm{mm}$, and $h_2 = 35\,\mathrm{mm}$. $l_1 = 0$ to l ($= 0.8\,\mathrm{m}$).

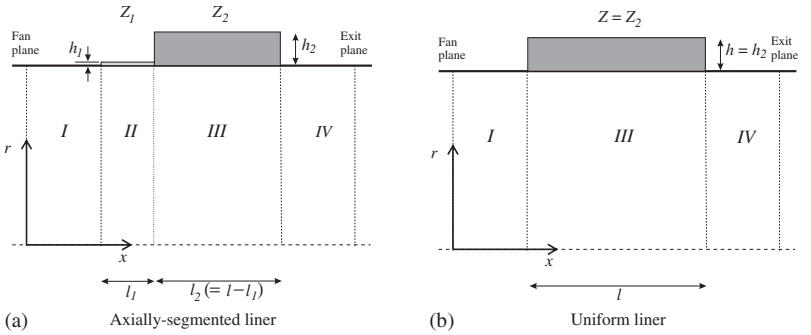

Fig. 7. Inlet duct geometry. Comparison of the axially segmented and uniform liner designs.

Table 3
Predicted sound power transmission loss at blade passing frequency

Sideline fan speed Flow condition—duct liner	Δ_{PWL} Mode-matching (dB)	Δ_{PWL} Finite element method (dB)
No flow—uniform liner	26.6	26.6
No flow—'axial' liner	20.4	20.4
Uniform flow—uniform liner	13.1	13.4
Uniform flow—'axial' liner	38.1	39.9

4.3. Validation of mode matching by the finite element method

To assess the accuracy of the mode-matching technique, the acoustic field in the duct was simulated also by using ACTRAN/AE, a finite/infinite element code produced by Free Field Technologies.[8] Details of the method are given in Ref. [6]. A particular feature of ACTRAN/AE which makes it suitable for this type of duct acoustics problem is that the boundary conditions can be specified in terms of modes.

Simulations have been conducted for the axially segmented and uniform liner designs, with and without mean flow. The results are in Table 3, and shown in Figs. 8–11. It is seen that without flow the agreement between mode-matching and the finite element method is excellent; see the predicted values of Δ_{PWL} in Table 3, and also examples of the predicted radial and wall acoustic pressure amplitudes plotted in Figs. 8 and 10. Note that without flow the predicted attenuation with the axially segmented liner is less than with the uniform liner. This is because without flow, mode $(B, 2)$ is in fact cut-off. Comparison of the results without flow is included to demonstrate the accuracy of the mode-matching.

The inclusion of a uniform mean-flow affects slightly the accuracy of the comparison between mode-matching and the finite element method. The predicted values of Δ_{PWL} listed in Table 3 are not in exact agreement, although the comparison is still good. Fig. 9 shows examples of the radial pressure at each matching station. In general, there is close agreement between the two methods, apart from in Fig. 9(c). It is noted that with the axially segmented liner, Δ_{PWL} is nearly 40 dB, which means the acoustic pressure amplitude at the exit plane is only 1% of the pressure at the fan plane. Therefore, it is not surprising that the agreement between the two methods, seen in Fig. 9(c) at $x = d + l$, appears to be poor, because each plot of the radial pressure field has been normalized. In absolute terms, the pressure at $x = d + l$ (Fig. 9(c)) is about 1% of that at $x = d$ (Fig. 9(a)).

[8]Free Field Technologies S.A., 16 place de l'Université, B-1348 Louvain-la-Neuve, Belgium. http://www.fft.be info@fft.be

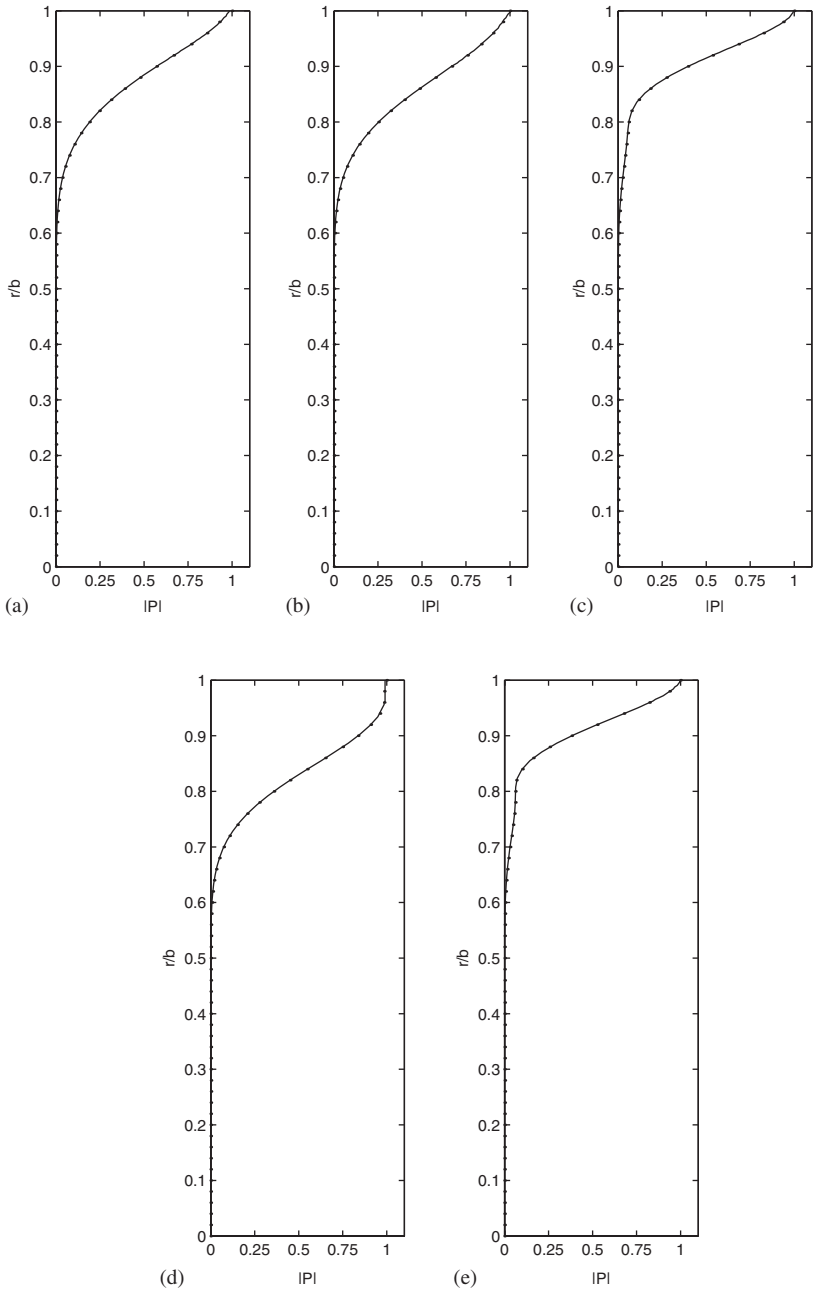

Fig. 8. Prediction of the radial acoustic pressure amplitude with no flow. Axially segmented liner: (a) $x = d$; (b) $x = d + l_1$; (c) $x = d + l_1 + l_2$ $(= d + l)$. Uniform liner: (d) $x = d$; (e) $x = d + l$. Key: •, mode-matching; —, finite element method.

Fig. 11 shows examples of the wall pressure. The agreement between the two methods is good, apart from at the matching stations. With a uniform flow, the finite element method predicts large wall pressure fluctuations which are localized at the matching stations. Koch and Möhring [20] examine a similar problem (finite length liner in a rectangle flow duct) using the Wiener–Hopf technique. They show that the solution is not unique. It depends on edge conditions applied at the liner's leading and trailing edge. In the Wiener–Hopf formulation, the jump in particle displacement at the edges of the liner is explicitly included in the solution. (Particle displacement at a rigid wall is zero, at an impedance wall it is non-zero.) Koch and Möhring demonstrate that

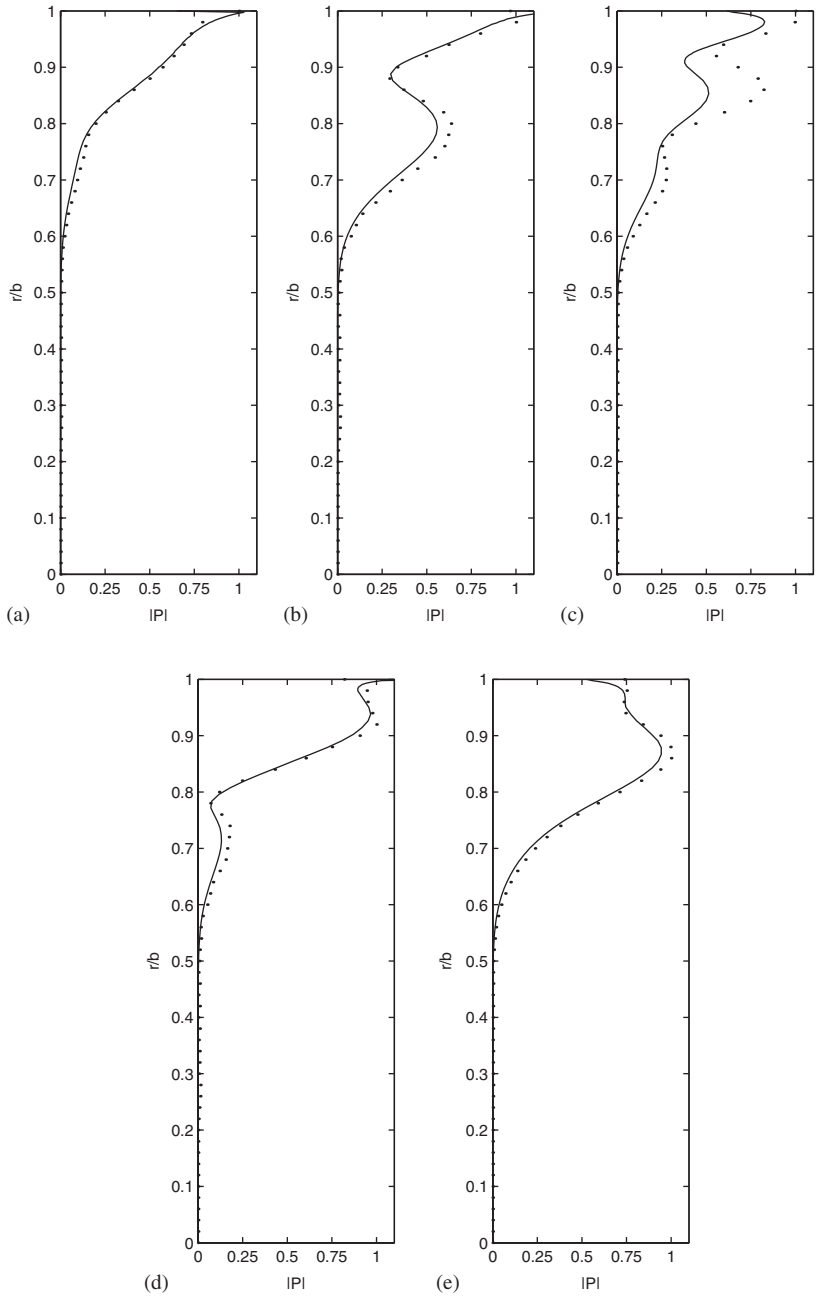

Fig. 9. Prediction of the radial acoustic pressure amplitude with uniform flow. Axially segmented liner: (a) $x = d$; (b) $x = d + l_1$; (c) $x = d + l_1 + l_2$ $(= d + l)$. Uniform liner: (d) $x = d$; (e) $x = d + l$. Key: •, mode-matching; —, finite element method.

the mode-matching technique corresponds to a Wiener–Hopf formulation with finite particle displacement jumps at the liner's leading and trailing edge. In this case, the pressure will be finite at the edges. One alternative Wiener–Hopf solution leads to a Kutta condition being satisfied at the leading edge, with singular behaviour at the trailing edge. (The use of a Kutta condition is linked to the instability mode.)

Although different edge conditions alter the Wiener–Hopf solution, Koch and Möhring found that the transmission coefficient was similar in each case. The different edge conditions mainly alter the value of the reflection coefficient. This is consistent with the comparison here between mode-matching and the finite

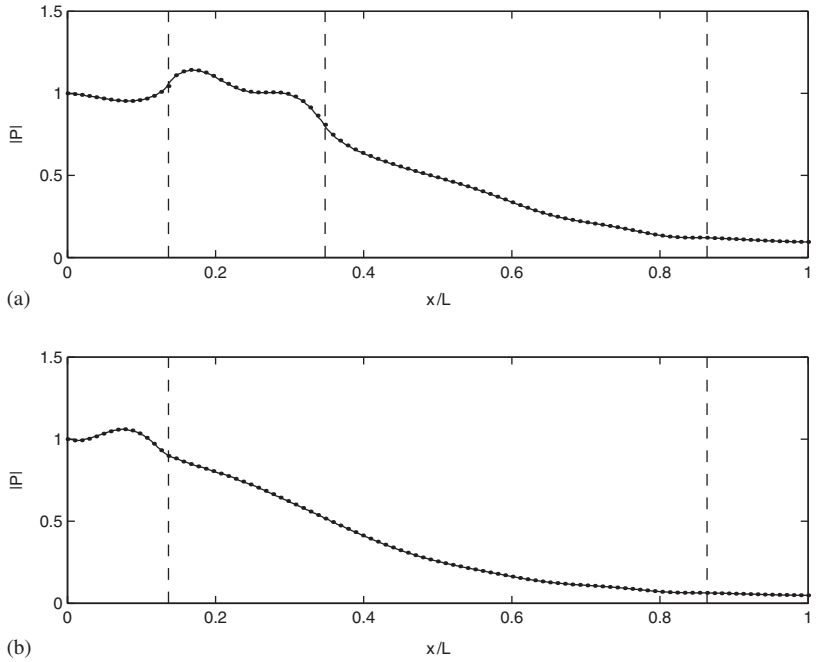

Fig. 10. Prediction of the acoustic pressure amplitude at the duct wall with no flow: (a) axially segmented liner; (b) uniform liner. Key: •, mode-matching; —, finite element method.

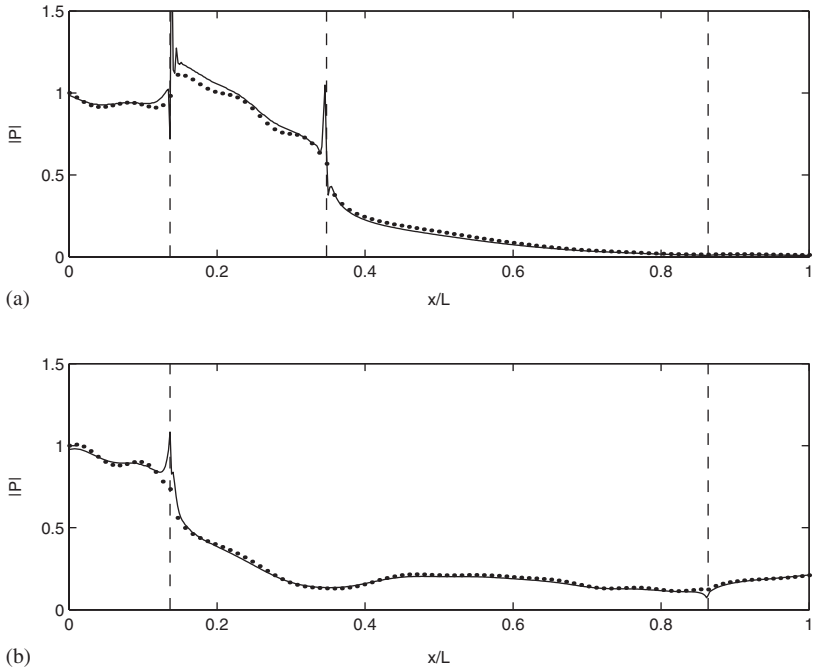

Fig. 11. Prediction of the acoustic pressure amplitude at the duct wall with uniform flow: (a) axially segmented liner; (b) uniform liner. Key: •, mode-matching; —, finite element method.

element method. The two methods predict similar sound power transmission losses, although the finite element results indicate the pressure at the duct wall may be singular at the matching stations. With the mode-matching procedure used here, although the boundary condition is discontinuous at the matching stations, the

Table 4
Radial wavenumbers (blade passing frequency)

Mode	$\kappa_{m,n}b$	$\mu^{+}_{m,n}b$	$\eta^{+}_{m,n}b$
$(B,1)$	$26.36+0.00\mathrm{i}$	$22.42+5.09\mathrm{i}$	$29.87+1.15\mathrm{i}$
$(B,2)$	$32.11+0.00\mathrm{i}$	$31.34+0.32\mathrm{i}$	$33.94+2.28\mathrm{i}$
$(B,3)$	$36.53+0.00\mathrm{i}$	$36.20+0.21\mathrm{i}$	$36.79+1.25\mathrm{i}$
$(B,4)$	$40.56+0.00\mathrm{i}$	$40.36+0.26\mathrm{i}$	$40.95+0.74\mathrm{i}$
$(B,5)$	$44.37+0.00\mathrm{i}$	$44.25+0.26\mathrm{i}$	$44.79+0.55\mathrm{i}$

κ, rigid duct; μ, lined duct $Z=Z_1=3-6.4\mathrm{i}$ (impedance of axially segmented liner—segment 1); η, lined duct $Z=Z_2=3-0.5\mathrm{i}$ (impedance of uniform liner, and axially segmented liner—segment 2).

Table 5
Axial wavenumbers (blade passing frequency)

Mode	$k_{x^{+}_{m,n}}b$	$\alpha_{x^{+}_{m,n}}b$	$\beta_{x^{+}_{m,n}}b$
$(B,1)$	$48.76-0.00\mathrm{i}$	$53.85-4.59\mathrm{i}$	$43.72-1.99\mathrm{i}$
$(B,2)$	$39.11-0.00\mathrm{i}$	$40.80-0.66\mathrm{i}$	$35.89-6.78\mathrm{i}$
$(B,3)$	$20.70-8.13\mathrm{i}$	$22.37-6.04\mathrm{i}$	$26.28-10.96\mathrm{i}$
$(B,4)$	$20.70-21.91\mathrm{i}$	$21.35-21.43\mathrm{i}$	$22.45-22.90\mathrm{i}$
$(B,5)$	$20.70-30.19\mathrm{i}$	$21.21-29.95\mathrm{i}$	$21.76-31.02\mathrm{i}$

k_x, rigid duct; α_x, lined duct $Z=Z_1=3-6.4\mathrm{i}$ (impedance of axially segmented liner—segment 1); β_x, lined duct $Z=Z_2=3-0.5\mathrm{i}$ (impedance of uniform liner, and axially segmented liner—segment 2).

pressure difference at each matching is minimized using the Galerkin method of weighted residuals. Thus, the type of large wall pressure fluctuations predicted using the finite element method are not predicted using this mode-matching formulation. In a forthcoming paper, Astley and Hii, using an alternative mode-matching formulation will demonstrate that the inclusion of additional terms in the matching (which account for the edge conditions with flow) leads to better agreement between mode matching and the finite element method.

5. Discussion

In this section the reasons for the prediction of a three-fold increase in the sound power transmission loss at BPF with the axially segmented liner compared with a typical uniform liner are outlined. Then, a detailed analysis of the results is in the following section, which uses an approximate mode-matching analysis to illustrate the key points in this discussion.

The axially segmented liner consists of a short length ($l_1=0.23\,\mathrm{m}$) of a thin cavity lining with resistance $R_1=3.0$, cavity depth $h_1=5\,\mathrm{mm}\Rightarrow Z_1=3-6.4\mathrm{i}$. This is joined to a thicker cavity lining with resistance $R_2=3.0$, cavity depth $h_1=35\,\mathrm{mm}\Rightarrow Z_2=3-0.5\mathrm{i}$. (The values of the specific acoustic impedance are at BPF.) The first five radial modes, associated with each type of duct section, are listed in Tables 4 and 5, and plotted in Figs. 12–14. In the rigid duct the first two radial mode orders are cut-on.[9]

With the thin lining ($Z=Z_1$), the radial wavenumber $\mu_{B,1}$ has a relatively large imaginary part compared with the higher mode orders. Rienstra [16] has shown that a mode which has a radial wavenumber with a large imaginary part will decay exponentially with distance away from the duct wall. This type of mode is known as a surface wave, because most of the acoustic energy is concentrated at the duct wall. This type of mode also

[9]Compare the axial decay rates of the cut-off modes in the rigid duct with the decay rates of these modes in the lined ducts. Modes $(B,3)$, $(B,4)$ and $(B,5)$ have similar decay rates in each duct section. This justifies the use of the term cut-off to refer to modes in both the rigid and lined duct sections.

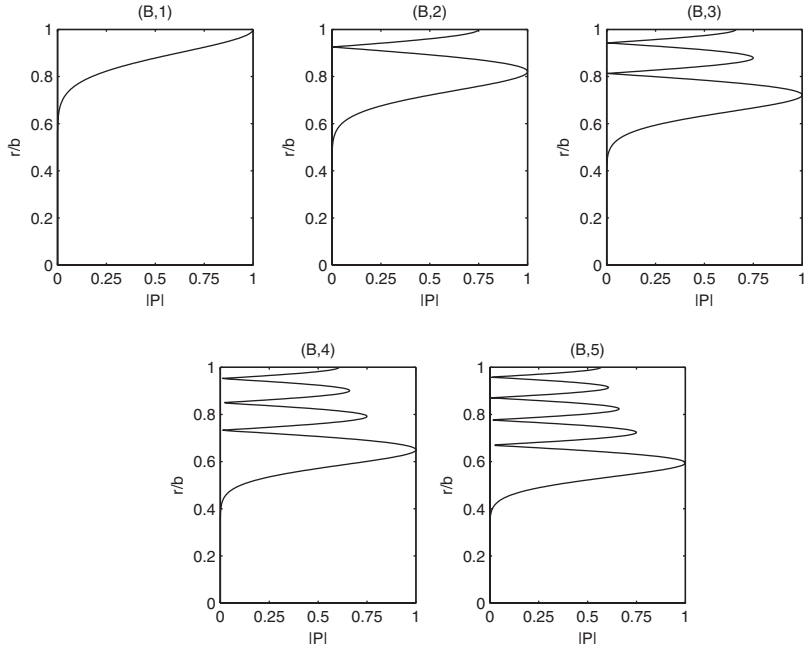

Fig. 12. Rigid duct mode shapes.

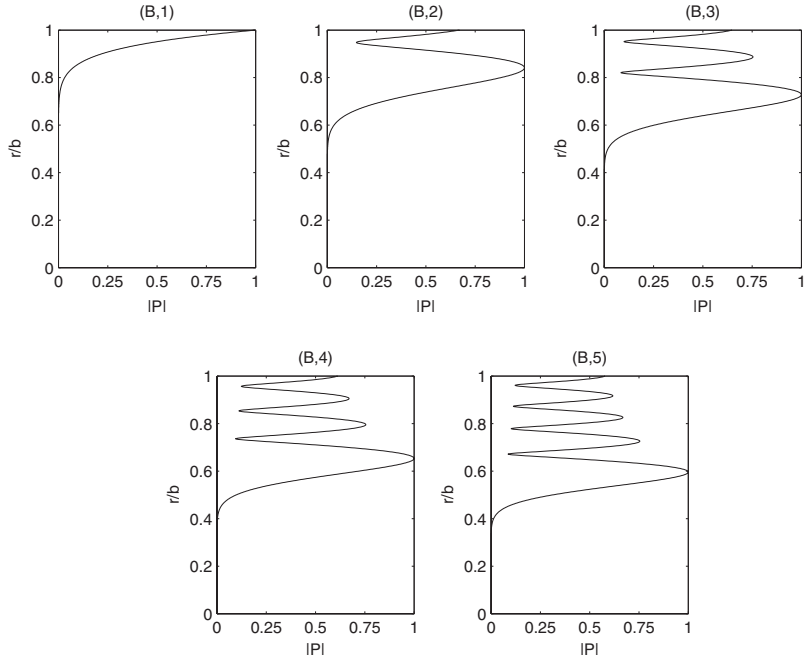

Fig. 13. Lined duct mode shapes. Specific acoustic impedance $Z = Z_1 = 3 - 6.4\mathrm{i}$. (Impedance of axially segmented liner—segment 1.)

tends to decay rapidly in the axial direction. With $Z = Z_1$, mode $(B, 1)$ resembles a surface wave; mode $(B, 2)$ is the least attenuated mode in this case.

With the thick lining ($Z = Z_2$) none of the modes resemble a surface wave. In this case, mode $(B, 1)$ is the least attenuated mode. Also, this mode has a higher axial decay rate, compared with the least attenuated mode with the thin lining, i.e. $\mathrm{Im}\{\beta_{x_{B,1}}^{+}\} > \mathrm{Im}\{\alpha_{x_{B,2}}^{+}\}$, because this lining is thicker.

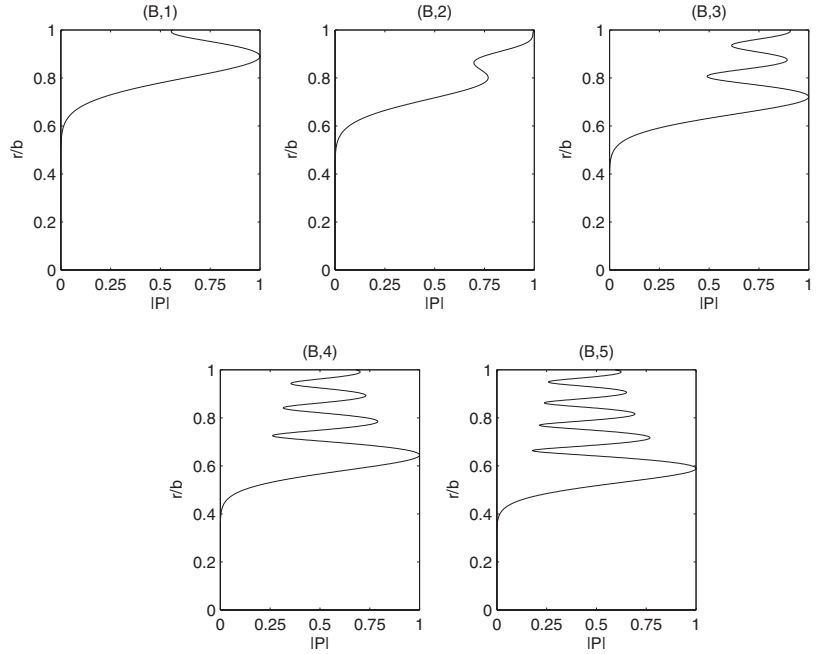

Fig. 14. Lined duct mode shapes. Specific acoustic impedance $Z = Z_2 = 3 - 0.5\mathrm{i}$. (Impedance of uniform liner, and axially segmented liner—segment 2.)

In order to assess the axially segmented liner, it is convenient to assume that the sound power transmission loss can be expressed, approximately, as

$$\Delta_{\mathrm{PWL}} \approx \Delta_{\mathrm{PWL}_1} + \Delta_{\mathrm{PWL}_2}, \tag{21}$$

where Δ_{PWL_1} and Δ_{PWL_2} are estimates of the transmission loss due to the first and second lined duct sections, respectively.

Estimates of Δ_{PWL_1} and Δ_{PWL_2} could be determined based on the attenuation of the least attenuated modes. This would neglect the other modes, and the effect of any scattering. These estimates are given by

$$\Delta_{\mathrm{LAM}_1} = -20\,\mathrm{Im}\{\alpha^{+}_{x_{B,2}}\} l_1 \log_{10} \mathrm{e}, \tag{22}$$

$$\Delta_{\mathrm{LAM}_2} = -20\,\mathrm{Im}\{\beta^{+}_{x_{B,1}}\} l_2 \log_{10} \mathrm{e}. \tag{23}$$

Note that in practice Eqs. (22) and (23) are normally applied when the lengths l_1, l_2 are sufficiently long, so that the energy transmitted by the other modes is negligible. In fact, the predicted transmission loss with the axially segmented liner significantly exceeds the estimate given by $\Delta_{\mathrm{LAM}_1} + \Delta_{\mathrm{LAM}_2}$. Now estimates of the transmission losses, Δ_{PWL_1} and Δ_{PWL_2}, due to each of the lined duct sections, are quantified separately.

Consider the first lined segment. Compare the mode shapes (shown plotted in Figs. 12 and 13) for the rigid duct, and the lined duct with impedance Z_1. The mode shapes are similar. Therefore, it would be anticipated that transmission of the rigid duct mode $(B, 1)$, at $x = d$, should scatter a significant proportion of the acoustic energy into the lined duct mode $(B, 1)$. Mode $(B, 1)$ is not the least attenuated mode when $Z = Z_1$, so the transmission loss Δ_{PWL_1} will exceed Δ_{LAM_1}.

Now consider the second lined segment. Compare the mode shapes (shown plotted in Figs. 13 and 14) for the two lined ducts with impedances Z_1 and Z_2. The modes shapes are less similar, notably the cut-on modes $(n = 1, 2)$. Therefore, in general, it would be anticipated that the transmission of the modes, at $x = d + l_1$, should scatter a proportion of the acoustic energy into the lined duct mode $(B, 1)$ in the second lined segment. In which case, because mode $(B, 1)$ is the least attenuated mode when $Z = Z_2$, the transmission loss Δ_{PWL_2} may

be close to Δ_{LAM_2}. However, in this case the first lined segment is also utilized as a scatterer.[10] The length l_1 is optimized, so that the acoustic energy scattered at $x = d + l_1$ into mode $(B, 1)$ is minimized. Then it follows that the transmission loss Δ_{PWL_2} will exceed Δ_{LAM_2}.

In summary, with the axially segmented liner, the transmission losses due to each lined duct section exceed the losses given by the axial decay rates of the least attenuated modes, i.e. $\Delta_{\mathrm{PWL}_1} > \Delta_{\mathrm{LAM}_1}$ and $\Delta_{\mathrm{PWL}_2} > \Delta_{\mathrm{LAM}_2}$. The combined effect leads to a three-fold increase in the overall sound power transmission loss at BPF compared with a typical uniform liner.

6. Analysis of results

In order to examine different types of axially segmented and uniform liners, an approximate mode-matching analysis is used. Simple estimates of the sound power transmission loss can be derived, to a first approximation, by neglecting: (1) cut-off modes; (2) left-running (reflected) modes in the lined duct sections. The use of (2) is based on the assumption that only the reflection at the liner's leading edge is significant. (This controls the reflected sound power.) At the end of each lined duct section, because the transmitted modes have been attenuated, the acoustic energy in the reflected modes is assumed to be small, and is omitted in the following analysis.

In the problem examined in this article only two radial modes are cut-on. It follows that the sound power transmission loss, Eq. (19), reduces to

$$\Delta_{\mathrm{PWL}} = 10\log_{10}\left(\frac{|A_{B,1}^{\mathrm{I}+}|^2\chi_{B,1}^{+} + |A_{B,2}^{\mathrm{I}+}|^2\chi_{B,2}^{+}}{|A_{B,1}^{\mathrm{IV}+}|^2\chi_{B,1}^{+} + |A_{B,2}^{\mathrm{IV}+}|^2\chi_{B,2}^{+}}\right). \tag{24}$$

Using assumptions (1) and (2), the mode-matching scheme given by Eqs. (13)–(15) reduces to:

$$\begin{bmatrix} A_{B,1}^{\mathrm{IV}+} \\ A_{B,2}^{\mathrm{IV}+} \end{bmatrix} \approx \begin{pmatrix} T_{11}^{3} & T_{12}^{3} \\ T_{21}^{3} & T_{22}^{3} \end{pmatrix} \begin{pmatrix} \mathrm{e}^{-\mathrm{i}\beta_{x_{B,1}^{+}}l_2} & 0 \\ 0 & \mathrm{e}^{-\mathrm{i}\beta_{x_{B,2}^{+}}l_2} \end{pmatrix} \begin{bmatrix} A_{B,1}^{\mathrm{III}+} \\ A_{B,2}^{\mathrm{III}+} \end{bmatrix}, \tag{25}$$

$$\begin{bmatrix} A_{B,1}^{\mathrm{III}+} \\ A_{B,2}^{\mathrm{III}+} \end{bmatrix} \approx \begin{pmatrix} T_{11}^{2} & T_{12}^{2} \\ T_{21}^{2} & T_{22}^{2} \end{pmatrix} \begin{pmatrix} \mathrm{e}^{-\mathrm{i}\alpha_{x_{B,1}^{+}}l_1} & 0 \\ 0 & \mathrm{e}^{-\mathrm{i}\alpha_{x_{B,2}^{+}}l_1} \end{pmatrix} \begin{bmatrix} A_{B,1}^{\mathrm{II}+} \\ A_{B,2}^{\mathrm{II}+} \end{bmatrix}, \tag{26}$$

$$\begin{bmatrix} A_{B,1}^{\mathrm{II}+} \\ A_{B,2}^{\mathrm{II}+} \end{bmatrix} \approx \begin{pmatrix} T_{11}^{1} & T_{12}^{1} \\ T_{21}^{1} & T_{22}^{1} \end{pmatrix} \begin{pmatrix} \mathrm{e}^{-\mathrm{i}k_{x_{B,1}^{+}}d} & 0 \\ 0 & \mathrm{e}^{-\mathrm{i}k_{x_{B,2}^{+}}d} \end{pmatrix} \begin{bmatrix} A_{B,1}^{\mathrm{I}+} \\ A_{B,2}^{\mathrm{I}+} \end{bmatrix}. \tag{27}$$

Also, in this analysis it is assumed that

$$\begin{bmatrix} A_{B,1}^{\mathrm{I}+} \\ A_{B,2}^{\mathrm{I}+} \end{bmatrix} = \begin{bmatrix} 1 \\ 0 \end{bmatrix}. \tag{28}$$

Combining Eqs. (26)–(28) gives

$$A_{B,1}^{\mathrm{II}+} \approx T_{11}^{1}\mathrm{e}^{-\mathrm{i}k_{x_{m,1}^{+}}d}, \tag{29}$$

$$A_{B,2}^{\mathrm{II}+} \approx T_{21}^{1}\mathrm{e}^{-\mathrm{i}k_{x_{m,1}^{+}}d}, \tag{30}$$

$$A_{B,1}^{\mathrm{III}+} \approx T_{11}^{2}T_{11}^{1}\mathrm{e}^{-\mathrm{i}\alpha_{x_{m,1}^{+}}l_1}\mathrm{e}^{-\mathrm{i}k_{x_{m,1}^{+}}d} + T_{12}^{2}T_{21}^{1}\mathrm{e}^{-\mathrm{i}\alpha_{x_{m,2}^{+}}l_1}\mathrm{e}^{-\mathrm{i}k_{x_{m,1}^{+}}d}, \tag{31}$$

$$A_{B,2}^{\mathrm{III}+} \approx T_{21}^{2}T_{11}^{1}\mathrm{e}^{-\mathrm{i}\alpha_{x_{m,1}^{+}}l_1}\mathrm{e}^{-\mathrm{i}k_{x_{m,1}^{+}}d} + T_{22}^{2}T_{21}^{1}\mathrm{e}^{-\mathrm{i}\alpha_{x_{m,2}^{+}}l_1}\mathrm{e}^{-\mathrm{i}k_{x_{m,1}^{+}}d}. \tag{32}$$

Also, combining Eqs. (25), (31), (32) leads to expressions for $A_{B,1}^{\mathrm{IV}+}$ and $A_{B,2}^{\mathrm{IV}+}$.

[10] In addition to absorbing some of the acoustic energy.

Eq. (25) also can be used to formulate simple estimates for Δ_{PWL}, based on setting $A^{\mathrm{III}+}_{B,2}=0$ or $A^{\mathrm{III}+}_{B,1}=0$:

$$A^{\mathrm{III}+}_{B,2}=0 \rightarrow \Delta_{\mathrm{PWL}\,n=1} \approx -20\,\mathrm{Im}\{\beta_{x\,B,1}^{+}\}l_2\log_{10}\mathrm{e}-20\log_{10}|A^{\mathrm{III}+}_{B,1}|+C_1, \tag{33}$$

$$A^{\mathrm{III}+}_{B,1}=0 \rightarrow \Delta_{\mathrm{PWL}\,n=2} \approx -20\,\mathrm{Im}\{\beta_{x\,B,2}^{+}\}l_2\log_{10}\mathrm{e}-20\log_{10}|A^{\mathrm{III}+}_{B,2}|+C_2, \tag{34}$$

where

$$C_1=10\log_{10}\chi^{+}_{B,1}-10\log_{10}(|T^{3}_{11}|^2\chi^{+}_{B,1}+|T^{3}_{21}|^2\chi^{+}_{B,2}), \tag{35}$$

$$C_2=10\log_{10}\chi^{+}_{B,1}-10\log_{10}(|T^{3}_{12}|^2\chi^{+}_{B,1}+|T^{3}_{22}|^2\chi^{+}_{B,2}). \tag{36}$$

Eqs. (33) and (34) are estimates of Δ_{PWL}, if *all* the acoustic energy is scattered into mode $(B,1)$ or mode $(B,2)$ in the second lined duct section (III). This means $A^{\mathrm{III}+}_{B,2}=0$ or $A^{\mathrm{III}+}_{B,1}=0$, respectively. For $l_2\gg 1$, then one of Eqs. (33) or (34) should be a good estimate of Δ_{PWL}. This depends whether $(B,1)$ or $(B,2)$ is the least attenuated mode.

Note that for a uniform liner, lined duct section II is omitted in the analysis. In this case

$$A^{\mathrm{III}+}_{B,2}=0 \rightarrow \Delta_{\mathrm{PWL}\,n=1} \approx -20\,\mathrm{Im}\{\beta_{x\,B,1}^{+}\}l\log_{10}\mathrm{e}-20\log_{10}|A^{\mathrm{III}+}_{B,1}|+C_1, \tag{37}$$

$$A^{\mathrm{III}+}_{B,1}=0 \rightarrow \Delta_{\mathrm{PWL}\,n=2} \approx -20\,\mathrm{Im}\{\beta_{x\,B,2}^{+}\}l\log_{10}\mathrm{e}-20\log_{10}|A^{\mathrm{III}+}_{B,2}|+C_2. \tag{38}$$

Note: for a uniform liner $A^{\mathrm{III}+}_{B,1}$ and $A^{\mathrm{III}+}_{B,2}$ are the same as $A^{\mathrm{II}+}_{B,1}$ and $A^{\mathrm{II}+}_{B,2}$ for an axial liner, given by Eqs. (29), and (30).

This approximate mode-matching analysis provides different estimates of the sound power transmission loss, if all the acoustic energy is scattered into a single mode (in the lined duct section III). Eqs. (33) and (34) apply to an axially segmented liner, and Eqs. (37) and (38) apply to a uniform liner. These estimates are now compared against results from the full mode-matching technique. First, the two different acoustic impedances (Z_1 and Z_2) are considered individually, in order to determine the transmission loss in a uniformly lined duct when each type of lining is used separately. Then, several different configurations of a two-section axially segmented lined duct are considered, in order to determine how changing length l_1 affects the transmission loss.

First, two different uniformly lined ducts are examined, having specific acoustic impedance Z_1 or Z_2. Fig. 15 shows how Δ_{PWL} varies with liner length l, for $l=0$ to 4 m. Results are shown for liner lengths up to $l=4$ m, in order to examine the value of Δ_{PWL} for large l. Also plotted are $\Delta_{\mathrm{PWL}\,n=1}$ and $\Delta_{\mathrm{PWL}\,n=2}$.

Consider the thin cavity lining with impedance $Z=Z_1$. In Fig. 15(a), for $l>0.5$ m, $\Delta_{\mathrm{PWL}}\approx\Delta_{\mathrm{PWL}\,n=2}$. Mode $(B,2)$ is the least attenuated mode. However, for $l<0.5$ m a better estimate of Δ_{PWL} is given by $\Delta_{\mathrm{PWL}\,n=1}$. Mode $(B,1)$ is not the least attenuated mode, but owing to the similarity of the mode shapes in the rigid and lined duct, a significant proportion of the acoustic energy is scattered into this mode. Accordingly, for short lengths of this lining the rate of attenuation is greater than the decay rate of the least attenuated mode.

Now consider the thicker cavity lining with impedance $Z=Z_2$. In Fig. 15(b), in general, $\Delta_{\mathrm{PWL}}\approx\Delta_{\mathrm{PWL}\,n=1}$ for all l. The attenuation is determined by the least attenuated mode, which is mode $(B,1)$ in this case.

Now compare the two linings. For short liner lengths, the transmission loss predicted with the thin lining is higher. This suggests that a short length of the thin lining could be beneficial, but the length of this lining is crucial.

Now several different two-section axially segmented liners are examined. Each of the liners has a different fixed length of thin lining (l_1). In Fig. 16(a)–(d), Δ_{PWL} is plotted for four different axially segmented liners with $l_1=0.1$, 0.2, 0.3 and 0.4 m, respectively. In each case, the plots show how Δ_{PWL} varies with liner length l_2, for $l_2=0-4$ m. Also plotted are $\Delta_{\mathrm{PWL}\,n=1}$ and $\Delta_{\mathrm{PWL}\,n=2}$.

In Fig. 16(a,c,d), it can be seen that Eq. (33) provides a good estimate of Δ_{PWL} for an axially segmented liner when $l_1=0.1, 0.2$ and 0.4 m. Compare Eqs. (21) and (33). This leads to

$$\Delta_{\mathrm{PWL}}\approx \underbrace{-20\log_{10}|A^{\mathrm{III}+}_{B,1}|+C_1}_{\Delta_{\mathrm{PWL}_1}}\underbrace{-20\,\mathrm{Im}\left\{\beta_{x\,B,1}^{+}\right\}l_2\log_{10}\mathrm{e}}_{\Delta_{\mathrm{PWL}_2}}, \tag{39}$$

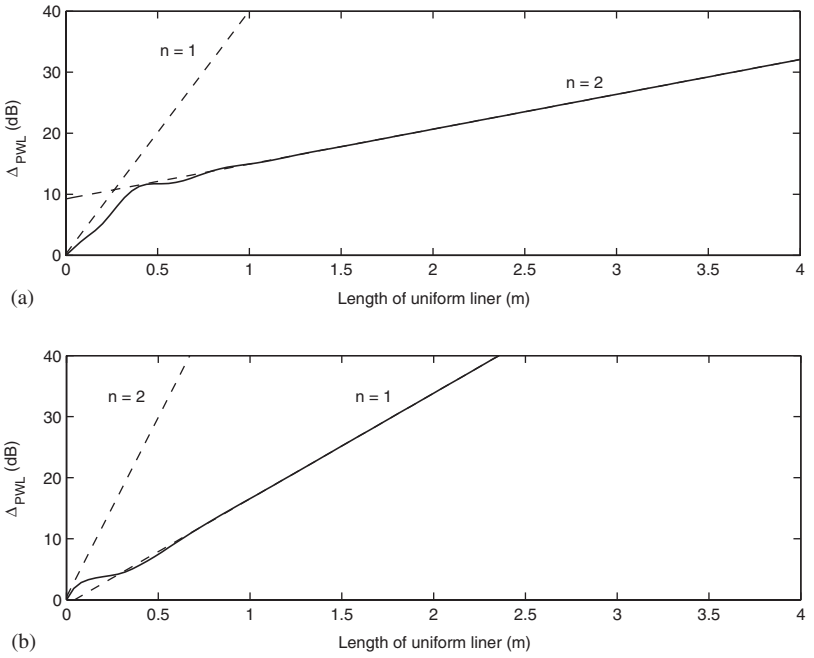

Fig. 15. Examples of the predicted sound power transmission loss at blade passing frequency for two different uniform liners. The variation of Δ_{PWL} with liner length is shown, (for $l = 0-4$m). Specific acoustic impedance of the lining is: (a) $Z = Z_1 = 3 - 6.4\mathrm{i}$. (Impedance of axially segmented liner—segment 1.) (b) $Z = Z_2 = 3 - 0.5\mathrm{i}$. (Impedance of uniform liner, and axially segmented liner—segment 2.) Key: —, Δ_{PWL}; - - -, $\Delta_{\mathrm{PWL}\,n=1,2}$.

i.e.

$$\Delta_{\mathrm{PWL}}(l_2) \approx \Delta_{\mathrm{PWL}_1} - 20\,\mathrm{Im}\{\beta_{x_{B,1}^+}\} l_2 \log_{10} \mathrm{e}. \tag{40}$$

The attenuation in the second lined duct segment is determined by the decay rate $\mathrm{Im}\{\beta_{x_{B,1}^+}\}$ of the least attenuated mode.

Now examine Fig. 16(b) when $l_1 = 0.2$ m. For $l_2 > 0.3$ m, $\Delta_{\mathrm{PWL}} \approx \Delta_{\mathrm{PWL}\,n=1}$. However, for $l_2 < 0.3$ m a better estimate of Δ_{PWL} is given by $\Delta_{\mathrm{PWL}\,n=2}$. In this case, the attenuation in the second lined duct segment is determined by the decay rate $\mathrm{Im}\{\beta_{x_{B,2}^+}\}$, which is not the least attenuated mode. Consequently, the attenuation due to the second lined duct section is increased when $l_1 = 0.2$ m.

The optimum length of the thin lining can be deduced. In Section 4, Fig. 6 shows how Δ_{PWL} varies with l_1, when $l = 0.8$ m (fixed). Compare Fig. 6 with Fig. 17, which shows how $|A^{\mathrm{II}+}|$ and $|A^{\mathrm{III}+}|$, for modes $(B, 1)$ and $(B, 2)$, vary with l_1. In Fig. 17, the values of $|A^{\mathrm{II}+}|$ and $|A^{\mathrm{III}+}|$ have been calculated by using mode-matching, and also approximately using Eqs. (29)–(32). Note the close agreement between the mode-matching results and the estimated values of the modal amplitudes.

For modes $(B, 1)$ and $(B, 2)$, $|A^{\mathrm{II}+}|$ is approximately constant, so the modal amplitudes in the first lined duct segment are independent of its length. The modal amplitude $|A_{B,1}^{\mathrm{II}+}| > |A_{B,2}^{\mathrm{II}+}|$, so there is a significant proportion of the energy scattered into the first radial mode, although this is not the least attenuated mode in the first lined duct section.

The values of $|A_{B,1}^{\mathrm{III}+}|$ and $|A_{B,2}^{\mathrm{III}+}|$ depend on scattering between the first and second lined duct segments. The optimum length of the scatterer (first lined duct section) is the value of l_1 which minimizes the acoustic energy scattered into the least attenuated mode in the second lined duct section. This is equivalent to minimizing $|A_{B,1}^{\mathrm{III}+}|$, which can be deduced from Eq. (31). In Fig. 17(b) it is seen that $|A_{B,1}^{\mathrm{III}+}|$ is minimized when l_1 is about 0.23 m. This is the same length as the optimum value of l_1, seen in Fig. 6, which maximizes Δ_{PWL}.

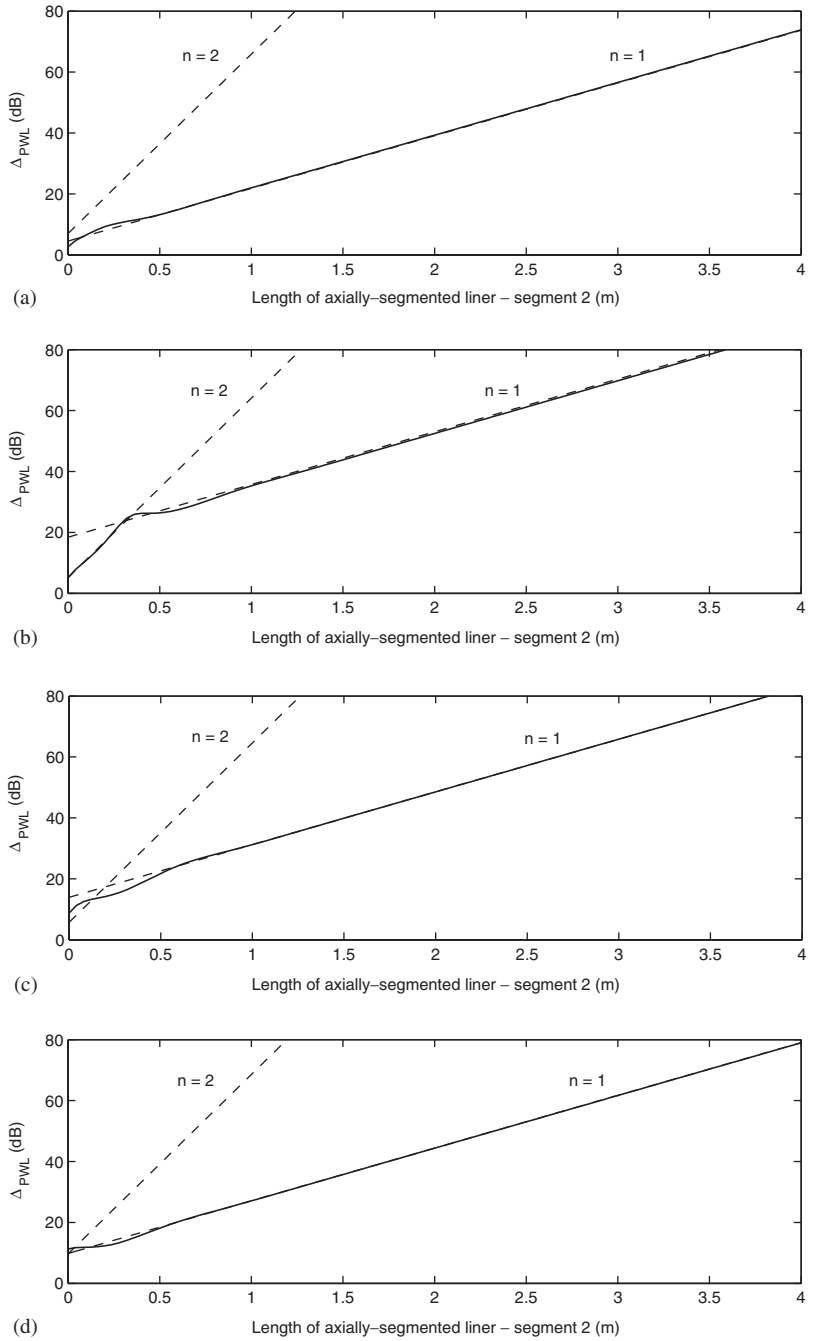

Fig. 16. Examples of the predicted sound power transmission loss at blade passing frequency for four different axial liners. The variation of Δ_{PWL} with length l_2 is shown, (for $l_2 = 0-4$ m). Specific acoustic impedance of the linings is $Z_1 = 3 - 6.4i$ and $Z_2 = 3 - 0.5i$. In each case, length l_1 is fixed: (a) $l_1 = 0.1$ m; (b) $l_1 = 0.2$ m; (c) $l_1 = 0.3$ m; (d) $l_1 = 0.4$ m. Key: —, Δ_{PWL}; - - -, $\Delta_{PWL\,n=1,2}$.

7. Conclusions

The aim of the type of axially segmented liner proposed in this article is to increase the attenuation of fan tones at high engine powers. In this article, the liner's design has been optimized based on a single mode—rotor-alone EO mode $(B, 1)$—which is used to model the BPF tone at high supersonic fan speeds. In practice,

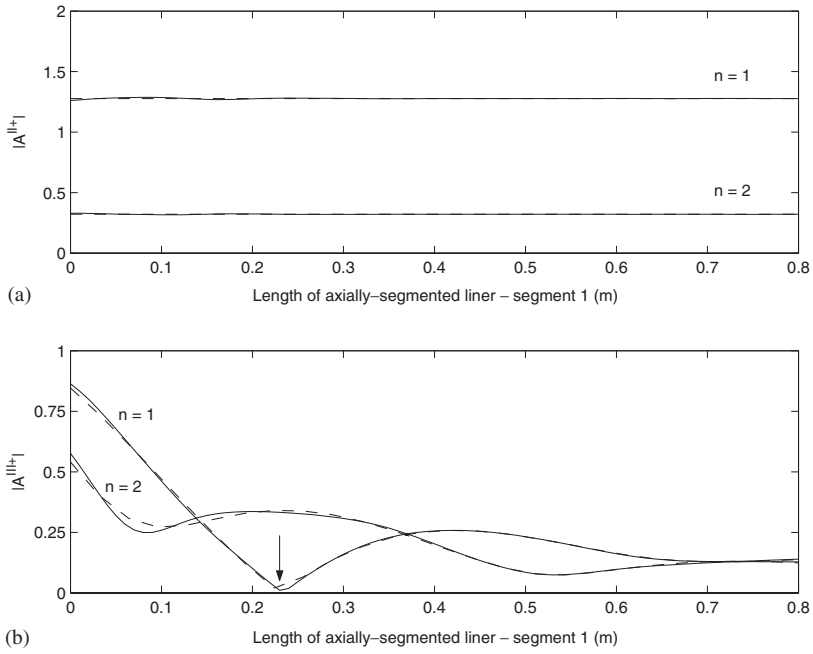

Fig. 17. Predicted values of the modal amplitudes, ($|A^{\mathrm{II}+}|$ and $|A^{\mathrm{III}+}|$), with the axially segmented liner. Modes (B, n), $n = 1$ and 2, at blade passing frequency, are shown. Specific acoustic impedance of the linings is $Z_1 = 3 - 6.4\mathrm{i}$ and $Z_2 = 3 - 0.5\mathrm{i}$: (a) variation of $|A^{\mathrm{II}+}|$ with length l_1; (b) variation of $|A^{\mathrm{III}+}|$ with length l_1. In each case l is fixed, $l_1 = 0{-}0.8$ m, and $l_2 = l - l_1$. Amplitudes of radial mode orders $n = 1$ and 2 are shown. The optimum length of liner l_1, which minimizes $A^{\mathrm{III}+}_{B,1}$, is shown by the vertical arrow. Key: —, Δ_{PWL}; - - -, $\Delta_{\mathrm{PWL}\,n=1,2}$.

the design of any inlet duct liner will be based on the attenuation of various tonal and broadband noise sources, at different fan speeds. Fig. 18 shows the predicted sound power transmission loss for rotor-alone EO modes $(m, 1)$ for $m = 1$ to $4B$, i.e. frequencies up to $4 \times$ BPF. Predictions for the axially segmented and uniform liner designs are shown. Compare the predicted values of Δ_{PWL} with the two types of liner. Although this axially segmented liner design has been only optimized at BPF, for the frequency range $17 < \mathrm{EO} < 70$, the predicted transmission loss is higher with the axially segmented liner. This suggests that it may be possible to design a more practical type of axially segmented liner, by finding the optimal design based on a range of frequencies.

At subsonic fan speeds the rotor-alone modes are cut-off, and at low supersonic fan speeds the rotor-alone modes are near cut-off. An axially segmented liner is unlikely to be of benefit at these fan speeds because less radial modes are cut-on; also, at these lower engine powers the modes are more easily attenuated anyway.

In this article sound power transmission losses have been calculated based on a source consisting of a single mode. A recent paper by Zlavog and Eversman [21] demonstrates that if the source consists of two or more radial modes of similar amplitude, then the transmission loss will depend on the relative phasing of these modes. It has been assumed that the energy in the rotor-alone source (at the fan plane) is confined to the first radial mode order. It is likely that higher radial mode orders generated at the fan plane will have lower amplitudes than the first radial mode, but a source consisting of more than one mode could be prescribed to examine how this would affect the predicted transmission loss with an axially segmented liner.

In the problem examined in this article only two radial modes are cut-on at BPF. The two-section axially segmented liner is designed to scatter energy from radial mode order $n = 1$ to $n = 2$. If more than two modes are cut-on, then more than two lined segments may be required to scatter energy into the higher radial mode orders. However, with more lined duct sections this could also cause energy to be scattered back into low radial mode orders.

Planned future work includes a more complex axially segmented liner optimization study which will include the use of a multi-mode source, and search over a prescribed frequency range. A preliminary attempt at such

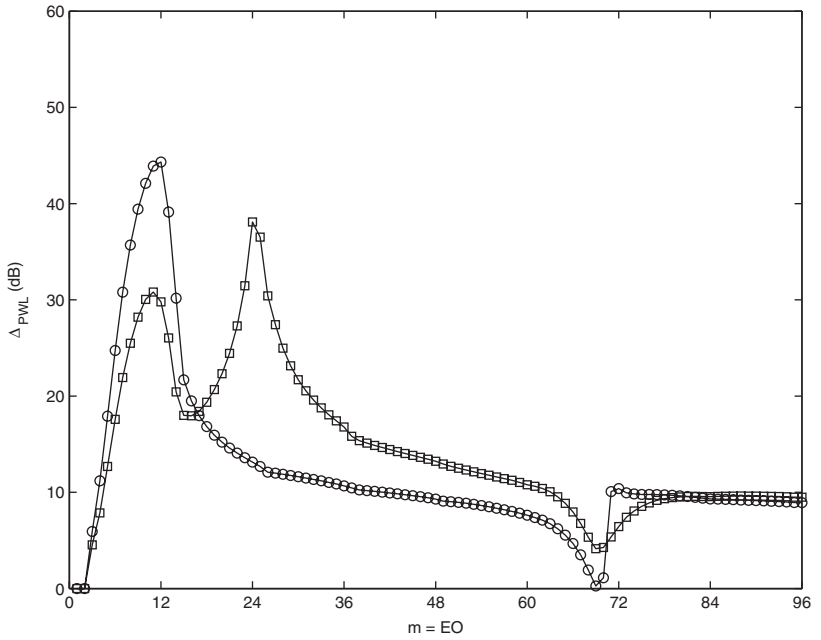

Fig. 18. Predicted sound power transmission losses for rotor-alone tones $m = \mathrm{EO}$. Key: ○, uniform liner; □, axially segmented liner.

an approach is reported in Ref. [19]. Also, the concept of a two-section axially segmented liner will be extended to a multi-section axially segmented liner. The aim is to analyse a single-mode, single-frequency source, to examine whether the optimum number of lined duct sections should equal the number of cut-on radial mode orders.

A passive axially segmented liner would be relatively straightforward to manufacture and install in a turbofan inlet duct. Alternatively, perhaps the best way to make use of this concept would be to have an adaptive scattering liner, although this technology has not yet been demonstrated for use in a real turbofan inlet duct.

Acknowledgements

Part of this work was funded by the European 5th framework "Technology Platform" SILENCE(R). AM, RJA and VJTH wish to acknowledge the continuing financial support provided by Rolls–Royce plc.

Appendix A. Transfer matrices T^1, T^2 and T^3

T^1, T^2 and T^3 are $(2N \times 2N)$ square matrices:

$$T^1 = \left(\begin{array}{c|c} c^+ & -a \\ \hline d^+ & -b^- \end{array}\right)^{-1} \left(\begin{array}{c|c} a & -c^- \\ \hline b^+ & -d^- \end{array}\right), \tag{41}$$

$$T^2 = \left(\begin{array}{c|c} e^+ & -c^- \\ \hline f^+ & -d^- \end{array}\right)^{-1} \left(\begin{array}{c|c} c^+ & -e^- \\ \hline d^+ & -f^- \end{array}\right), \tag{42}$$

$$T^3 = \left(\begin{array}{c|c} a & -e^- \\ \hline b^+ & -f^- \end{array}\right)^{-1} \left(\begin{array}{c|c} e^+ & -a \\ \hline f^+ & -b^- \end{array}\right), \tag{43}$$

where $a, b^{\pm}, c^{\pm}, d^{\pm}, e^{\pm}, f^{\pm}$ are each $(N\times N)$ square matrices. Element (i,j) of $a, b^{\pm}, c^{\pm}, d^{\pm}, e^{\pm}, f^{\pm}$ are,

$$a_{ij} = \int_{r=0}^{b} rJ_m(\kappa_{m,i}r)\, J_m(\kappa_{m,j}r)\, \mathrm{d}r, \tag{44}$$

$$b_{ij}^{\pm} = \frac{k_{x_{m,j}^{\pm}} a_{ij}}{\rho_0 c_0 (k - k_{x_{m,j}^{\pm}} M_x)}, \tag{45}$$

$$c_{ij}^{\pm} = \int_{r=0}^{b} rJ_m(\kappa_{m,i}r) J_m(\mu_{m,j}^{\pm}r)\, \mathrm{d}r, \tag{46}$$

$$d_{ij}^{\pm} = \frac{\alpha_{x_{m,j}^{\pm}} c_{ij}^{\pm}}{\rho_0 c_0 (k - \alpha_{x_{m,j}^{\pm}} M_x)}, \tag{47}$$

$$e_{ij}^{\pm} = \int_{r=0}^{b} rJ_m(\kappa_{m,i}r) J_m(\eta_{m,j}^{\pm}r)\, \mathrm{d}r, \tag{48}$$

$$f_{ij}^{\pm} = \frac{\beta_{x_{m,j}^{\pm}} e_{ij}^{\pm}}{\rho_0 c_0 (k - \beta_{x_{m,j}^{\pm}} M_x)}. \tag{49}$$

The integrals in Eqs. (44), (46), and (48) can be evaluated analytically:

$$\int_{r=0}^{b} rJ_m(\kappa_{m,i}r) J_m(\kappa_{m,j}r)\, \mathrm{d}r = \begin{cases} \dfrac{b^2}{2}\left[1 - \left(\dfrac{m}{\kappa_{m,i}b}\right)^2\right] J_m^2(\kappa_{m,i}b), & i = j, \\ 0, & i \neq j, \end{cases} \tag{50}$$

$$\int_{r=0}^{b} rJ_m(\kappa_{m,i}r) J_m(\mu_{m,j}^{\pm}r)\, \mathrm{d}r = \frac{b}{\kappa_{m,i}^2 - \mu_{m,j}^{\pm 2}} \left[\kappa_{m,i} J_{m+1}(\kappa_{m,i}b) J_m(\mu_{m,j}^{\pm}b) - \mu_{m,j}^{\pm} J_m(\kappa_{m,i}b) J_{m+1}(\mu_{m,j}^{\pm}b)\right], \tag{51}$$

$$\int_{r=0}^{b} rJ_m(\kappa_{m,i}r) J_m(\eta_{m,j}^{\pm}r)\, \mathrm{d}r = \frac{b}{\kappa_{m,i}^2 - \eta_{m,j}^{\pm 2}} \left[\kappa_{m,i} J_{m+1}(\kappa_{m,i}b) J_m(\eta_{m,j}^{\pm}b) - \eta_{m,j}^{\pm} J_m(\kappa_{m,i}b) J_{m+1}(\eta_{m,j}^{\pm}b)\right]. \tag{52}$$

Appendix B. Diagonal matrices D^1, D^2 and D^3

D^1, D^2 and D^3 are $(2N\times 2N)$ diagonal matrices:

$$D_{\mathrm{ii}}^{1} = \begin{array}{ll} \mathrm{e}^{-\mathrm{i}k_{x_{m,i}^{+}}d}, & i = 1 \,..\, N \\ \mathrm{e}^{\mathrm{i}\alpha_{x_{m,i}^{-}}l_1}, & i = N+1 \,..\, 2N \end{array} \tag{53}$$

$$D^2_{\mathrm{ii}} = \left.\begin{array}{ll} \mathrm{e}^{-\mathrm{i}\alpha_{x^+_{m,i}} l_1}, & i = 1 \,..\, N \\ \mathrm{e}^{\mathrm{i}\beta_{x^-_{m,i}} l_2}, & i = N+1 \,..\, 2N \end{array}\right\} \tag{54}$$

$$D^3_{\mathrm{ii}} = \left.\begin{array}{ll} \mathrm{e}^{-\mathrm{i}\beta_{x^+_{m,i}} l_2}, & i = 1 \,..\, N \\ \mathrm{e}^{\mathrm{i}k_{x^-_{m,i}} d}, & i = N+1 \,..\, 2N \end{array}\right\} \tag{55}$$

Appendix C. Calculation of modes in an acoustically lined circular-section duct

A modal solution of the convected Helmholtz equation (1) will be of the form

$$\hat{p}_{m,n}(r,\theta,x) = A_{m,n} J_m(\kappa_{m,n} r)\, \mathrm{e}^{\mathrm{i}(m\theta - k_{x_{m,n}} x)}. \tag{56}$$

The boundary condition for a circular-section duct of radius b with a locally reacting wall with (non-dimensional) specific acoustic impedance Z is

$$\frac{\partial \hat{p}}{\partial r} = -\frac{\mathrm{i}k}{Z}\left(1 - \frac{\mathrm{i}M_x}{k}\frac{\partial}{\partial x}\right)^2 \hat{p} \quad \text{at } r = b. \tag{57}$$

Combine Eqs. (56) and (57) to form the eigenvalue problem:

$$\kappa_{m,n} b\, \frac{J'_m(\kappa_{m,n} b)}{J_m(\kappa_{m,n} b)} = -\mathrm{i}\,\frac{kb}{Z}\left(1 - M_x\,\frac{k_x}{k}\right)^2. \tag{58}$$

In a rigid duct, the values of κ are found by solving

$$J'_m(\kappa_{m,n} b) = 0. \tag{59}$$

A tracking method, proposed by Eversman [1], is used to find the values of $\kappa_{m,n}$ in a lined duct. These are found by starting from the values in a rigid duct, and tracking the values of the κ's in the complex plane as the acoustic admittance is varied from zero (rigid wall) to $1/Z$ (lined wall, impedance Z). The tracking is performed using an initial value problem formulation, and the eigenvalues are refined using the Newton–Raphson method.

References

[1] W. Eversman, Theoretical models for duct acoustic propagation and radiation, *In Aeroacoustics of Flight Vehicles*: *Theory and Practice Vol. 2 Noise Control*, *NASA RP-1258*, 1991, pp. 101–163.

[2] W. Eversman, R.J. Beckemeyer, Transmission of sound in ducts with thin shear layers—convergence to the uniform flow case, *Journal of the Acoustical Society of America* 52 (1) (1972) 216–220.

[3] J.M. Tyler, T.G. Sofrin, Axial flow compressor noise studies, *SAE Transactions* 70 (1962) 309–332.

[4] S.W. Rienstra, Sound transmission in slowly varying circular and annular lined ducts with flow, *Journal of Fluid Mechanics* 380 (1999) 279–296.

[5] R.J. Astley, W. Eversman, A finite element formulation of the eigenvalue problem in lined ducts with flow, *Journal of Sound and Vibration* 65 (1) (1979) 61–74.

[6] A. McAlpine, M.C.M. Wright, Acoustic scattering by a spliced turbofan inlet duct liner at supersonic fan speeds, *Journal of Sound and Vibration* 292 (3–5) (2006) 911–934.

[7] D.L. Lansing, W.E. Zorumski, Effects of wall admittance changes on duct transmission and radiation of sound, *Journal of Sound and Vibration* 27 (1) (1973) 85–100.

[8] J.F. Unruh, Finite length tuning for low-frequency lining design, *Journal of Sound and Vibration* 45 (1) (1976) 5–14.

[9] K.J. Baumeister, Evaluation of optimized multisectioned acoustic liners, *AIAA Journal* 17 (11) (1979) 1185–1192.

[10] M.S. Tsai, Mode scatterer design for fan noise suppression in two-dimensional ducts, *Journal of Sound and Vibration* 83 (4) (1982) 501–512.

[11] N.J. Baker, A.J. Kempton, R.J. Astley, A. McAlpine, Acoustic liner for gas turbine engine, European Patent Number EP1411225, 2004.

[12] C.J. Chapman, Sound radiation from a cylindrical duct. Part 1. Ray structure of the duct modes and of the external field, *Journal of Fluid Mechanics* 281 (1994) 293–311.

[13] E.J. Rice, M.F. Heidmann, T.G. Sofrin, Modal propagation angles in a cylindrical duct with flow and their relation to sound radiation, AIAA 79-0183, 1979.

[14] E.J. Rice, Acoustic liner optimum impedance for spinning modes with mode cut-off ratio as the design criterion, AIAA 76-516, 1976.
[15] R. Mittra, S.W. Lee, Analytical Techniques in the Theory of Guided Waves, MacMillan Series in Electrical Science, 1971.
[16] S.W. Rienstra, A classification of duct modes based on surface waves, *Wave Motion* 1107 (2002) 1–17.
[17] A. Cummings, High frequency ray acoustics models for duct silencers, *Journal of Sound and Vibration* 221 (4) (1999) 681–708.
[18] C.L. Morfey, Sound transmission and generation in ducts with flow, *Journal of Sound and Vibration* 14 (1971) 37–55.
[19] L. Lafronza, A. McAlpine, A.J. Keane, R.J. Astley, Computer-aided liner optimization for broadband noise, AIAA 2004-3029, 2004.
[20] W. Koch, W. Möhring, Eigensolutions for liners in uniform mean flow ducts, *AIAA Journal* 21 (2) (1983) 200–213.
[21] G. Zlavog, W. Eversman, Source effects on realized attenuation in lined ducts, AIAA 2003-3247, 2003.